THE BOEING COMPANY
Aero-Space Division

IDENTIFYING OPTIMUM PARAMETERS OF HOT EXTRUSIONS

Contract NAS 7-276

Prepared for

Chief, Materials Research Branch
National Aeronautics & Space Administration
Headquarters
Washington, D. C.

Progress Report No. 3
Oct. 20, 1964 to Jan. 11, 1965

THE BOEING COMPANY
Aero-Space Division

IDENTIFYING OPTIMUM PARAMETERS OF HOT EXTRUSIONS

Contract NAS 7-276

Prepared for

Chief, Materials Research Branch
National Aeronautics & Space Administration
Headquarters
Washington, D. C.

Progress Report No. 3
Oct. 20, 1964 to Jan. 11, 1965

ABSTRACT

19865

The purpose of this program is to develop a technique for hot extruding MgO and to determine the effect of hot extrusion on MgO with preliminary evaluations on other oxide bodies. Two more canned extrusions of MgO and its alloys have been completed. CeO_2 billets were successfully fabricated by isostatic pressing. Problems attributed to gas entrapment in MgO fabrication occurred, but modifications of pressing procedures are resolving these. Another uncanned extrusion was made with better results.

Extrusion analysis shows that cracking should be reduced by slower cooling and relieving constraining of the ceramic by the can. Original large grain boundaries approximately parallel to the extrusion axis apparently slide during extrusion and result in preferential crack sites. Substantial grain elongation occurs during extrusion. The extruded body is nearly completely recrystallized giving a grain size much smaller than just prior to extrusion, and in fact smaller than in the starting billet. Very large grains are reduced much more than smaller ones, but do not produce as small an extruded grain size as a body of much smaller starting grain size. Dense MgO, MgO-NiO, and $MgO-Al_2O_3$ bodies show similar extrusion grain size, and highly oriented texture. MgO-CaO and $MgO-ZrO_2$ bodies are much more resistant to high temperature deformation. Increasing the extrusion temperature from 2100°C to 2400°C did not significantly change grain size, orientation, or densification in MgO, MgO-NiO, or $MgO-Al_2O_3$ bodies. The distribution of alloy agents is generally more homogenous after extrusion, but there is evidence of some grain boundary accumulation of alloy agents in $MgO-ZrO_2$, MgO-CaO, and $MgO-Al_2O_3$ bodies. Contamination from the Tungsten cans appears to be negligible.

Author

1

CONTENTS

ILLUSTRATIONS

TABLES

WORK ACCOMPLISHED

A.   BILLET FABRICATION

Data on billets 1.5" in diameter and generally about 1" long made during this period is summarized in Table 1. The fused MgO billets were ground from the same fully dense ingot* used throughout these experiments. The spinel was a sample[2] from a commercial fusion*. The ZrO_2** billet is from the previously noted purchase [3] (and is 3" long). Fabrication details are given in the following sections.

1)   MgO

Billets M-1-19 through M-2-4 were fabricated in new graphite ("Graph-i-tite G") dies from the same lot and purchase of Fisher MgO previously used[3]. However, as noted in Table 1, problems of lamination, or die or ram breakage occurred. Examination showed that M-1-17, M-1-18, and M-1-20, also had some laminations, and denser ends than centers. During fabrication of M-1-17 through M-1-20 snapping noises (transmitted through the pressing train) were heard. These snaps were often accompanied by temporary 10 to 50% increases in absolute pressure in the vacuum chamber. Absolute pressure in the vacuum pressing chamber often temporarily increased from the order of 10×10^{-3} Torr to the order of .1 to .2 Torr upon release of the 5000 psi ram pressure on the specimen. Similar increases in absolute chamber pressure accompanied the die breakage in Table 1 and the "Fiberfrax" blanket used for die insulation was "blown-out" between the induction coils along with fine MgO fragments. Closer examination of the unused Fisher powder indicated it had lost some of its "fluffiness" though stored in glass jars with the lids sealed with plastic tape. These observations and past experiments all indicate that the problem is due to increased gas content trapped in the rapidly densifying billet.

Experimental pressings of thinner disks based on this "gas hypothesis" led to modifying Vacuum Hot Pressing Procedure B for billet M-2-4 by waiting until 1150°C (2100°F) to apply ram pressure, which was built up slowly over a period of about 20 minutes.

A new lot of Fisher MgO powder was received, and initial tests indicated some possible gas problem. Therefore, billet M-2-5 from this new lot, was pressed on a compromise pressure cycle: pressure applied at 925°C (1700°F) and gradually increased to 5000 psi at 1130°C (2050°F).

These modifications in pressing procedure produced billets of satisfactory to good density without laminations in the billets or breakage of dies.

  * Product of Muscle Shoals Electrochemical Corp.
 ** Product of Zirconium Corp. of America
*** Product of Basic Carbon Corp.

2) MgO - 5 w/o NiO

Billets M5N-1-1 and M5N-1-2 were fabricated from Mallinckrodt reagent MgO and Baker reagent NiO per Vacuum Hot Pressing Procedure A, except: the NiO was added with the LiF, vacuum was not used [1], and a pressure of 5000 psi was applied. M5N-1-1 showed structure previously identified as flattened gas bubbles thus explaining the lower density. This and the die breakage with M5N-1-2 are consistent with the "gas hypothesis" and past experience with similar bodies at Boeing.

3) MgO - 5 w/o Al_2O_3

Billet M5A-1-1 was hot pressed per Vacuum Hot Pressing Procedure B from Fisher MgO and Alon C milled 2 hours in benzene. Alon C was chosen to possibly give a finer distribution of the Al_2O_3 and for its expected higher reactivity.

4) MgO-2 w/o ZrO_2

Billet M2Z-1-6 was hot pressed from Fisher MgO and colloidal ZrO_2 milled in benzene prior to the above noted problems with MgO billets.

5) CaO

Billet C-1-4, from CaO made from $Ca(OH)_2$ per calcining Procedure A, was fabricated per Vacuum Hot Pressing Procedure B, except pressure was applied over a period of 15 minutes because of possible gas problems.

6) CeO_2

Billets Ce-1-1 and Ce-1-2 are from 1 rod of isostatically pressed (30,000 psi for 5 minutes with 10 minute pressure release) and fired Lindsay 99.9 +% CeO_2 [3]. Firing of this rod at 1315°C (2400°F) for 17 hours then later firing it to 1425°C (2600°F) for 14 hours resulted in densities repectively of 5.8 gm/cc and 6.64 gm/cc. A final firing at 1565°C (2850°F) for 14 hours, during which the rod broke approximately in half, resulted in densities of 6.62 gm/cc and 6.82 gm/cc in the two halves. Heating and cooling times were respectively 16 hours or more and 8 or more hours.

B. EXTRUSION

Extrusions are performed by Nuclear Metals, Incorporated, Concord, Mass. Selection and analysis of extrusions are made jointly by Boeing and Nuclear Metals.

1) Catch Tube

The carbon sections [3] for catch tube insulation withstood the mechanical stresses of catching the extrusion, and increased the cooling time approximately three fold. The extrusion now takes about three minutes to cool

below red heat.

The catch tube with these carbon sections was used for all extrusions analyzed in this report, and reduced occasional warping and bending of extrusions.

2)   Canned Extrusions

Two more extrusions of MgO and MgO alloy billets in tungsten cans have been completed. Data for these and the three similar extrusions completed just prior to the last report [3] is summarized in Table II. The order and composition of each ceramic billet in these extrusions is listed in Table III.

A typical break-down of an extrusion is shown in Fig. 1A and an unextruded tail illustrating the reduction and flow is shown in Fig. 1 B. Samples of the extrusions with half the can cut off are shown in Figs. 2 to 4. Billet mg-1 of extrusion MgO-6 was + 14 mesh 99.5 % pure – MgO fused grain.*

3)   Uncanned Extrusion

Another uncanned extrusion trial (see Fig. 5) similar to the last one (3) was made except the temperature was 2300°C instead of 2200°C and the 0.1" wall graphite lubricating sleeve was eliminated to use more conventional glass lubrication and to reduce graphite contamination. The die was filled with insulating fiberglass for lubrication since possible loss of the outer tantalum foil precluded rolling the hot billet through proprietary powdered glass lubricant during transfer to the extrusion press.

The TZM nose extruded uniformly, followed by a drop in pressure and an increase in speed during initial extrusion of the MgO. The pressure then rose and the MgO stalled after about 60% of the MgO extruded. About 1" of the MgO attached to the TZM nose remained in one piece (with 1 or more cracks), while the remainder of the extruded material which came out of the die fragmented. Many fragments often had dimensions between 0.5" and 1" – much larger than the pieces in the last attempt. The diameter of the MgO attached to the TZM nose was about 1.5" while the die exit is only about 1.25". This MgO on the TZM nose did not have the slight translucency of that in the die and adjoining fragments. The fragments showed no sign of the carbon contamination previously observed.

* Product of General Electric Co.

C.   MATERIAL ANALYSIS

1)   Extrusion Uniformity

Extruded ceramic billets frequently showed a maximum diameter shortly behind their tip as seen in Figures 2 to 4, (especially in billets M-f-3, MIA-1-8, and M4C-1-2). This bulbous nose was followed by a more uniform section where equilibrium flow had apparently been established.

Bulbous noses were not observed in the following billet when the tail of the preceding billet flowed over the nose of the following billet as seen in Fig. 2 (Billet M-1-12), Fig. 3 (Billet M-1-4), and Fig. 4 (Billet M2N-1-6). Very uniform transitions between billets are shown in Fig. 6.

These regions of apparent uniform flow usually varied some in diameter, with a given cross section commonly having differences in diameter of 5 to 10%. A range of samples of this variation is seen in Fig. 7 (see also Fig. 11 B and note Reduction Ratio variation in Table II). The position or magnitude of a maximum diameter would often gradually change along the extrusion axis (e.g. compare M2N-1-3 of Fig. 7 and in Fig. 6 A and B).

Minor protrusions of the can into the ceramic occurred with all billets fabricated from MgO grain prior to canning (see Fig. 2 - Billet MG-1, and Fig. 4 - Billet M G-2), but not in the MgO grain packed in the can Fig. 4 - Billet mg-1). Larger protrusions occurred with the fused billets M2Z-1-1 and M5C-1-2 (Fig. 3) but not with billet MION-1-1 whose surface porosity before extrusion was respectively greater than M5C-1-2 and M2Z-1-1 (see Fig. 8). An increase in the number and size of protrusions made it difficult or impossible to remove the ceramic billet from the can halves.

An extreme non-uniformity occurred near the end of billet M-f-4 (MgO-2) with the MgO actually coming out of the can as shown in Fig. 9. This section was preceded by another smaller non-uniformity and followed by a still smaller one. The first 50% or more of the specimen was typical of other similar extrusion, and the tail appeared to be again approaching equilibrium flow.

2)   Density

Definite densification occurred in some billets as shown by comparing densities before and after extrusion in Table III. This was particularly marked in the MgO-2 w/o NIO bodies which prior to extrusion showed little or no translucency in a thickness of 0.1 to 0.2", while substantial translucency was observed in all such billets after extrusion. Billets

8

MG-1, MG-2, and MG-3 fabricated from grain [3] prior to extrusion apparently also densified as indicated by a slight translucency and higher average reduction ratio (see Table III). (These densities were not measured because of difficulty of removing adequate sections from the can). Billet mg-1 showed extensive densification, and apparently was denser than MG-1 to 3. The transparency of billet M-1-7 in Fig. 7D which represents about average transparency for the dense MgO bodies indicates near theoretical density.

3)   Cracking

Two general types of cracking termed random and linear (since the intersection of the crack and a surface parallel or perpendicular to the extrusion axis is generally a reasonably straight line) are observed. Examples of random cracking are M2Z-1-1 and M5C-1-2 (Fig. 3), MG-2 (Fig. 10A) and MION-1-1 (Fig. 10B). A typical linear cracking example in the longitudinal section of M-1-11 is seen in Fig. 10 C, while examples in transverse sections are seen in Fig. 7. A possible intermediate case is seen in M4C-1-4 in Fig. 10 D.

Random cracks apparently originated from surface irregularities as seen in Fig. 10 A. Such cracking was characteristic of MgO fabricated from grain prior to extrusion and all billets from fused ingots (MION-1-1, M2Z-1-1, and M5C-1-2). Random cracking also occurred in the uncanned extrusion. Random cracking was of diminishing characterization of hot pressed MgO-2 w/o ZrO_2 (M2Z-1-3), hot pressed MgO-4 w/o - CaO (M4C-1-4, M4C-1-1, and M4C-1-2), and grain packed in the can (mg-1).

Linear cracking in general increased as random cracking decreased. However, the density of linear cracks was much less than random cracks as seen by contrasting Figs. 10 A and B with Figs. 7, 10 C and 10 D. The spacing of transverse linear cracks varied from 0.25" to 0.75". Linear cracking was characteristic of all dense hot pressed bodies of MgO, MgO-1 w/o Al_2O_3, and MgO - 2 w/o NiO except in extrusion MgO-1. There closer examination showed that billet MIA-1-1 was characterized mostly by linear cracking with some possible random cracking, while M2N-1-1 appeared to be characterized mostly by random cracking (very fine). These latter two billets had rougher surfaces (from minor can protrusions) than their counterparts in extrusions MgO-2, 3, and 6.

Transverse linear cracks (perpendicular to the extrusion axis) are generally quite planar, while longitudinal cracks (parallel to the extrusion axis) are sometimes more curved as seen in Fig. 7. Such longitudinal cracks generally appeared greater in number and often more distinct in MgO - 1 w/o Al_2O_3 than in MgO and MgO - 2 w/o NiO. (This is also true of MIA-1-1 in extrusion MgO-1).

9

Examination of Figs. 7 and 10 C will show that linear cracks generally stop shortly below the surface. This is substantiated by microscopic examination. It is also generally true that one linear crack intersecting another will result in the termination of one as shown in Fig. 10 C.

The above comments on linear cracking are generally true of the billets ground from the fused MgO ingot (M-f-3 through 5). However, there is substantial evidence that most longitudinal cracking in these is at or near the original grain boundaries that were generally oriented approximately parallel to the extrusion axis. Figs. 11 A and B show a fairly good correspondence between cracks in the extruded billet and the original grain boundaries. The main boundary dividing the original billet M-f-4 in half (Fig. 11 C) showed a distinct correspondence with a linear crack dividing the extruded body in half. Fig. 11 D is a sample of this crack surface which is corrugated or striated.

4)   Microstructure

Estimated grain sizes of the extruded bodies are given in Table III. Typical transverse sections (fractured at transverse linear cracks) are shown in Figs. 12 A, B and C, with the corresponding typical longitudinal sections shown in Figs. 12 D, E and F.* A surface rim of grains 30 to 60% of the average grain size as illustrated in Fig. 13, occurred on most specimens. The thickness of this rim was generally a few hundred microns thick, but sometimes reached a thickness of over 1000 microns – most often with MgO-2 $^W/_O$ NiO specimens. (This rim effect was not entered in the estimate of grain size). The least uniform grain sizes were in bodies of fused MgO or with MgO grain, where patches of different sized grains were found, sometimes showing extremes of grain size difference of the order of 50 fold. An especially distinct case is shown in Fig. 14. In the fused MgO bodies, there frequently appeared to be a difference in the average grain size between regions bounded by longitudinal linear cracks though there was significant variation within these regions. There also often appeared to be a reduced grain size along these longitudinal linear cracks in the fused MgO bodies. Generally the MgO-CaO and MgO-ZrO$_2$ bodies were most uniform in grain size. Several occurances of apparently unrecrystallized grains or outlines of elongated grains that had recrystallized (see Fig. 14 and 15) were found inside the above noted rim, but usually within 0.1" of the edge of the extrusion.

Grain size just prior to extrusion and the above variations in extruded grain size are necessary to evaluate the estimated grain sizes of Table III. Grain size prior to extrusion will depend upon time and temperature as

* All MgO and MgO alloy fracture surfaces were etched 5 to 10 seconds in concentrated boiling chromic acid to etch dislocations and boundaries. No differences in grain structure were found between cut and fractured surfaces. All cut surfaces were dry sanded as fine as 600 grit paper then etched 20 to 40 seconds in the boiling chromic acid.

well as composition and density (for example an increase of porosity from a fraction of a percent to about 2% can result in 3 fold reduction in grain size). Grain growth rate will decrease with increasing temperature above 1600 - 1800°C unless a grain growth inhibiting second phase is dissolved. Bodies of a smaller grain size will generally show a higher rate of growth than those of larger grain size under comparable conditions. These observations and studies allow the estimates of grain size before extrusion shown in Table IV to be made.

Microstructure shows that transverse fractures are predominantly cleavage as seen in Figs. 12 A, B, C, 13 A and B. These figures and the contrast in fracture surface flatness shown between an unextruded and an extruded fracture surface in Fig. 16 indicate substantial orientation in the extruded body. Longitudinal fracture surfaces were rougher and possibly contained less cleavage.

Etched fracture surfaces revealed a significant amount of formed or partially formed sub-boundaries in the MgO, MgO-NiO, and MgO-Al$_2$O$_3$ bodies as illustrated in Fig. 17. Comparison between Fig. 16 B and Figs. 16 A, 17, 12 A, B, C, and 13 show a higher dislocation density in the extruded bodies of MgO, than the unextruded body. General comparison indicated that there was a respective decrease in dislocation density in MgO, MgO-NiO, MgO-Al$_2$O$_3$, MgO-ZrO$_2$, and MgO-CaO bodies with the latter two being substantially lower than the first three.

5)   Second Phase Analysis

Electron probe examination of billet M5C-1-2 (MgO-4) showed some evidence of grain boundary accumulation of a CaO rich phase, but substantially less than reported for M5C-1-1 (MgO-1)[3]. There was distinct accumulation of a CaO rich phase at or near several cracks similar to that previously reported by Rice[4]. An estimate of the CaO concentration showed no significant loss of CaO from the body.

Similar examination of billet M4C-1-1 (MgO-4) shows a quite uniform distribution of CaO, and no apparent loss of CaO. Billet M4C-1-4 (MgO-4) showed some evidence of CaO accumulation at or near some grain boundaries and voids (or cracks).

The MgO - 2 $^w/_o$ ZrO$_2$ fused ingot, from which billet M2Z-1-1 was cut, frequently had ZrO$_2$ rich regions* of varying thickness around parts of grain boundaries, especially smaller grains as shown in Fig. 18 A. It also frequently contained 1 or more random ZrO$_2$ rich regions of the order of 5 microns within grains. Thin section analysis and electron microscope examination revealed a dense population of rods (see Fig. 18) oriented approximately in the {100} direction [4]. Electron probe analysis of

* The electron probe showed Ca, Hf, and Si in the ZrO$_2$ rich regions.

billet M2Z-1-1 after extrusion shows no distinct grain outlining as in Fig. 18 A, but an increase in the density and size of random ZrO_2 rich regions was observed. Electron microscope examination indicated substantial reduction in the density and uniformity of distribution and shape of the rods. Fabrication of billets, such as M2Z-1-3[3], from grain ground from this MgO - 2 $^w/o$ ZrO_2 ingot resulted in a body of agglomerated particles several microns in diameter with no rods distributed with in the grains. Electron probe examination of the extruded M2Z-1-3 billet showed a fairly uniform distribution of ZrO_2 rich regions a few microns in diameter with no indicated grain boundary accumulations as seen in Fig. 19 A. Electron micrographs of etched fracture surfaces frequently showed the structure seen in Fig. 19 B. Apparently much of this structure, which is suggestive of a second phase, occurred at grain boundaries. This examination also showed some regions of structure similar to the rods of Fig. 18 B.

Electron micrographs of fracture surfaces of extruded MgO-1 $^w/o$ Al_2O_3 bodies showed structure similar to that of Fig. 19 B. This structure was not found in MgO or MgO - 2 $^w/o$ NiO bodies.

Electron probe analysis of MgO - 2 $^w/o$ NiO bodies shows a generally uniform distribution of the NiO, except for a surface rim of a few hundred microns where there is little or no NiO.

Electron probe analysis for tungsten showed that many specimens have no tungsten, while other specimens show tungsten to depths up to several hundred microns. The tungsten always appears as small particles rather than a diffuse region, is sporadic and usually at quite a low concentration.

6) Orientation

The maximum orientation of many of the billets is shown in Table III. This was determined by comparing the peak intensity of the {200} plane on a transverse section with the same plane of a randomly oriented MgO body*. A high and low value of this maximum are also shown to indicate the degree of variations. Such variation is normally due to grain size differences, cracking, and non uniformity of the extrusion. Cursory trials indicated that extremes of surface preparation would make at most a 10 to 20% difference in such highly oriented bodies.

* Some of the values for extrusion MgO-1 are not in agreement with those given in the last report.[3] Further experimentation indicated discrepancies which now appear due to exceeding the counting efficiencies of the geiger detectors previously used. This has now been corrected by use of a scintillation counter. The qualitative nature of the MgO pole figure [3] would not be changed, but the quantitative values will be corrected.

DISCUSSION AND CONCLUSION

The variations in vacuum chamber pressure during hot pressing of MgO bodies that laminated, broke rams, or broke dies indicate gas entrapment in the rapidly densifying bodies. Previous experience at Boeing, observations on the powders, and successful fabrication by delayed and slower pressure application all corroborate this. However, further pressing procedure modification appears necessary to obtain the highest possible quality billets from the present powders.

Isostatic pressing and subsequent firing of reagent grade CeO_2 has produced suitable CeO_2 bodies. Modifications of the initial fabrication parameters should reduce the present 7% or less porosity achieved.

The elimination of the graphite lubricating sleeve on the uncanned extrusion gave more uniform extrusion, and grossly reduced graphite contamination. However, it appears that the fiberglass did not provide adequate lubrication – resulting in incomplete extrusion. Thin wall tubes or cans instead of foil covering would allow the use of lubrication procedures used in canned extrusion which should provide adequate lubrication. The discrepency between the diameter of the MgO attached to the TZM nose and the MgO in the die tail may be due to bloating caused by impurities. This fact, plus the generally inferior results of similar billets in canned extrusion indicates that billets of higher purity and density are needed for further progress with this technique.

Densification generally occurred during extrusion (the indicated lower density of M2Z-1-3 after extrusion could be due to cracking or experimental error) with billets of the highest density before extrusion having the highest density after extrusion. However, complete densification did not generally occur as shown by both density measurements and trans-lucency. Greater densification occurred in the high purity MgO grain (mg-1) just packed in the can than in the bodies fabricated with grain prior to extrusion. This is believed due primarily to the higher purity of mg-1 allowing easier, more homogenous flow, although intergranular sliding before complete bonding of grains may have helped.

The non-uniformities of the extrusions are due to changes in flow characteristics of the ceramic interacting with the flow characteristics of the can. Bulbous noses appear to be most likely when a stiffer material follows a softer one. Inhomogenities in billet flow characteristics or density as well as can inhomogenities will also contribute to these problems. Significant protrusions of the can into billets M2Z-1-1 and M5C-1-2 (MgO-4), but not into billet MION-1-1 appears to be due to the greater stiffness of the former two as shown by their lower reduction and higher extrusion pressure (even at a higher tempera-ture), and thus apparently allowing the tungsten to flow into the large surface pores. However, MION-1-1 was not as stiff, and therefore could apparently flow to close its substantial surface porosity.

The stresses in the cooling extruded body are complex and not completely known; however, the cracking patterns observed suggest some general mechanisms. Many of the longitudinal linear cracks are quite suggestive of failure observed in diametral – compression[5]. Similar compression would be expected to occur due to the can cooling faster than the ceramic, especially where the ceramic diameter was not uniform. The transverse linear cracking could result from longitudinal thermal stresses due to cooling along the extrusion combined with tensile stresses resulting from the low thermal expansion tungsten can gripping the higher expansion ceramic at relative maxima of the ceramics varying diameter.

13

Much of the random cracking also apparently results from such gripping of the ceramic by the can. However, this gripping does not appear to be the sole cause since random cracking was observed in MION-1-1, M2N-1-1, and the uncanned extrusion, all of which had relatively smooth surfaces and uniform diameters in a given cross section. Another possible source of such cracking would be radial compression of a cylindrical body with crack deflectors such as pores, second phases (ZrO_2 and CaO rich phases should be present during or shortly after extrusion), and poorly oriented grains. All of the bodies with random cracking appeared to have at least one of these characteristics.

All of these observations on cracking suggest that to prevent cracking stresses the extrusion must be cooled slower or the can must not restrain the ceramic contraction on cooling. Slower cooling will reduce constraining of the ceramic by the can as will obtaining more uniform ceramic extruded sections as by producing more uniform billets, longer billets, or higher reduction ratios (since this gives a longer extrusion). However, use of much thinner wall cans or cans with thin slots filled with a material (e.g. MgO powder) to prevent welding of the slots may also grossly reduce constraining by the can by fracture of the thin wall or slots respectively during cooling of the extrusion.

Original grain boundaries and longitudinal cracks in fused MgO bodies extruded with long grain boundaries approximately parallel to the extrusion axis appear to correspond quite well. The indicated general variation of grain size between sections bounded by these cracks and evidence of original boundaries previously presented [1] corroborate this. This would appear to be due to grain boundary sliding. The corrogated or striated surface seen on these cracks would appear to be due to the combination of longitudinal sliding along the boundary and the grain boundary corrogation of MgO during high temperature deformation recently reported by Day and Stokes [6].

Evidence demonstrates that substantial grain elongation occurs during extrusion as expected, but this rapidly recrystallizes - agreeing with observations on CaO [3]. However, the indication of a few remnant elongated grains, an apparently higher dislocation density, and partially formed substructure indicate that recrystallization is not quite complete.

Comparison of grain sizes between Tables III and IV clearly shows substantial reduction in grain size as previously reported [1]. Extruded grain size is also generally smaller than in the starting billet prior to heating for extrusion.

Measurements of orientation show that all dense MgO, MgO-NiO, and MgO-Al_2O_3 extruded bodies are highly oriented. This is corroborated by observations on cleavage fracture surface flatness.

The lower reduction ratio and higher extrusion force for the MgO-CaO and MgO-ZrO_2 bodies shows a much higher resistance to plastic flow. This may mean greater high temperature strengths in these bodies.

No significant differences were observed in bodies fabricated per Vacuum Hot Pressing Procedures A or B.

Contamination of the ceramic by the tungsten can appears to be minor. The tungsten observed in some bodies is believed to be carried in from the surface during sample preparation since it appears to occur as sporatic, discrete particles in dense bodies with no sign of diffusion.

Increasing the extrusion temperature from 2100°C to 2400°C did not appear to significantly effect grain size, densification, or orientation in the MgO, MgO-NiO, or MgO-Al_2O_3 bodies. It should however, improve extrusion of MgO-CaO and MgO-ZrO_2 bodies if billets of comparable flow characteristics are extruded together.

WORK IN PROGRESS AND PLANNED

A.   **Work In Progress**

An extrusion of CeO_2, fused $MgAl_2O_4$, CaO, and ZrO_2 (CaO stabilized) in a TZM can at 2000°C is now in preparation.

Further improvement in hot pressing procedure are being sought.

MgO bodies with 5 $^w/_o$ NiO or 5 $^w/_o$ Al_2O_3 are being prepared for comparisons with bodies of lower NiO and Al_2O_3 content.

B.   **Work Planned**

Plans are being made for one or two extrusions to investigate each of the following parameters:

1)   Higher reduction ratio to evaluate this effect on bodies and to obtain longer uniform extruded sections to reduce cracking.

2)   Cans with two diametrically opposite slots to reduce cracking by relieving can restraint on the ceramic.

3)   Thin wall cans to reduce can constraint, possible can non-uniformity, and resultant cracking.

REFERENCES

(1)   Progress Report 1, "Identifying Optimum Parameters of Hot Extrusions",
        Contract NAS 7-276, April 17th to July 13, 1964.

(2)   Obtained through the courtesy of Jimmie Ardis of Muscle Shoals Electromineral
        Corporation.

(3)   Progress Report 2, "Identifying Optimum Parameters of Hot Extrusions," Contract
        NAS 7-276, July 14 to October 19, 1964.

(4)   R. W. Rice, "Internal Surfaces In MgO", presented at the Conference on the
        Role of Grain Boundaries and Surfaces In Ceramics at Raleigh, N. C. In
        Nov., 1964, preceedings to be published.

(5)   A. Rudnick, A. R. Hunter, F. C. Holden, "An Analysis of the Diametral –
        Compression Test", Materials Research and Standards 3 (4) 283-288, April, 1963.

(6)   R. B. Day, R. J. Stokes, "Grain Boundaries and The Mechanical Behavior of
        Magnesium Oxide", Contract AF 33 (615) – 1282, Dec., 1964.
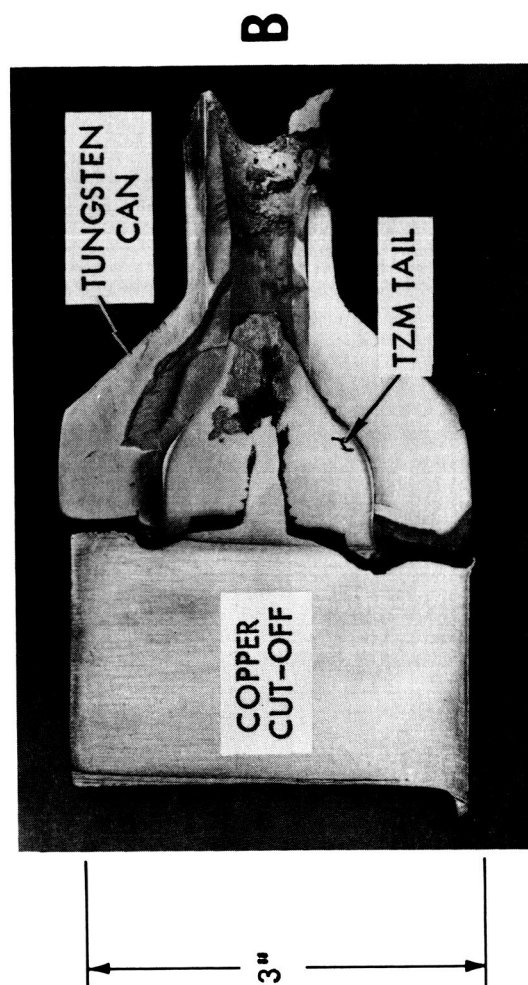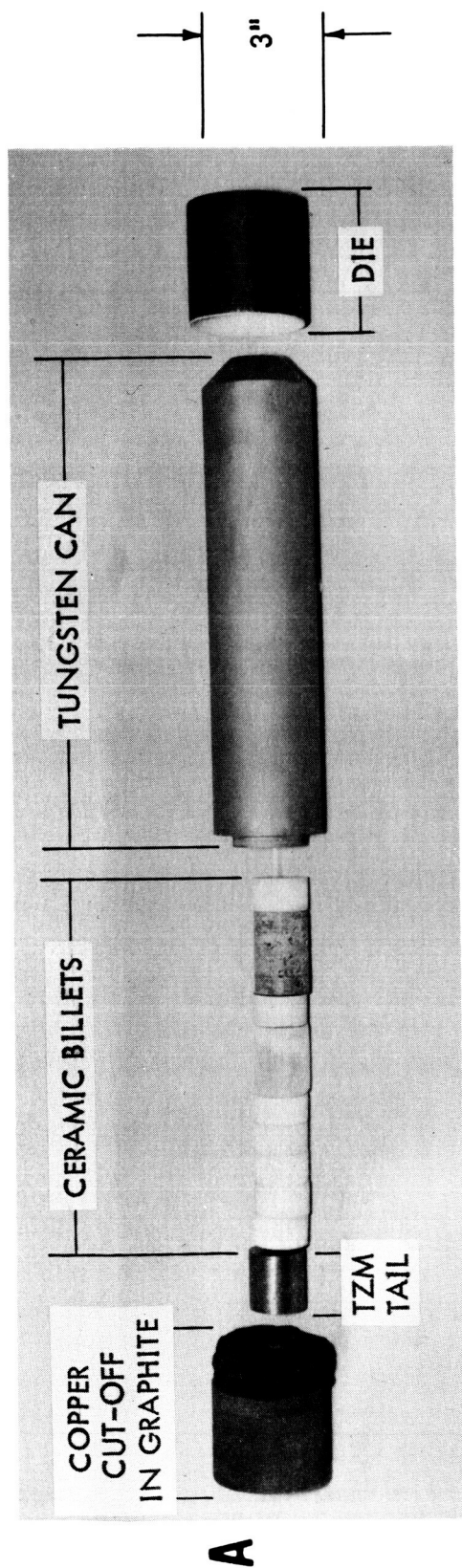
FIGURE 1   EXTRUSION BREAKDOWN AND REDUCTION.   A) BREAKDOWN OF COMPOSITE BILLET B) STALLED TAIL OF EXTRUSION MgO–2

FIGURE 2   EXTRUSION MgO-3 AND MgO-5 SAMPLES A) BILLET M-f-3 (MgO-3)
B) BILLET M-f-5 (MgO-5), C) TAIL OF BILLET MG-1 AND MOST OF
M-1-12 (FROM MgO-5)

19

NOSE

1" DIA.

M2Z-1-1

M2Z-1-3

M-1-4

M5C-1-2

M4C-1-1

M4C-1-4
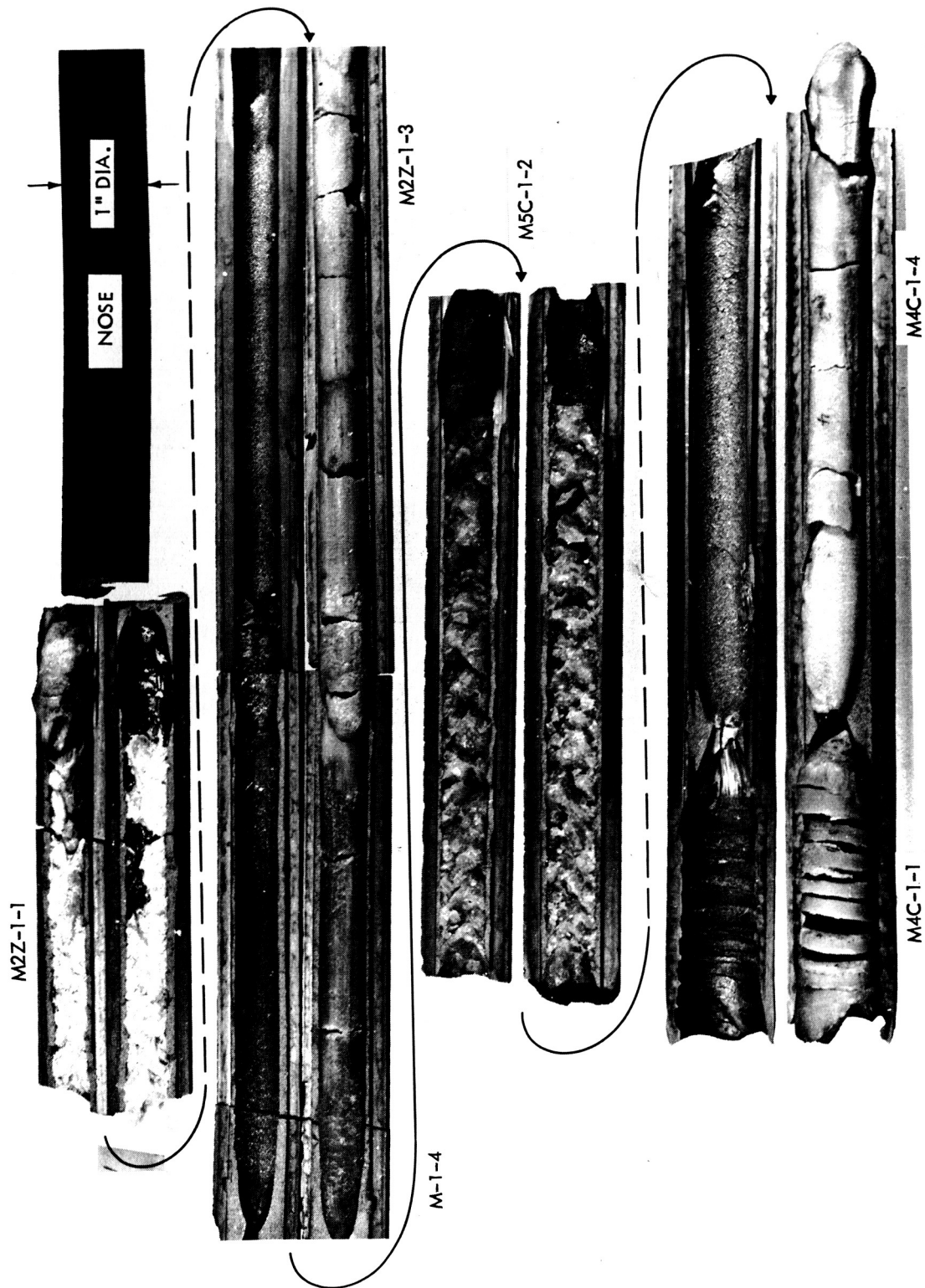
FIGURE 3   EXTRUSION MgO-4 SAMPLES

1" DIA.   NOSE

M2N-1-6

M-1-15

MIA-1-8

M2N-1-6

MG-2

M4C-1-2

mg-1
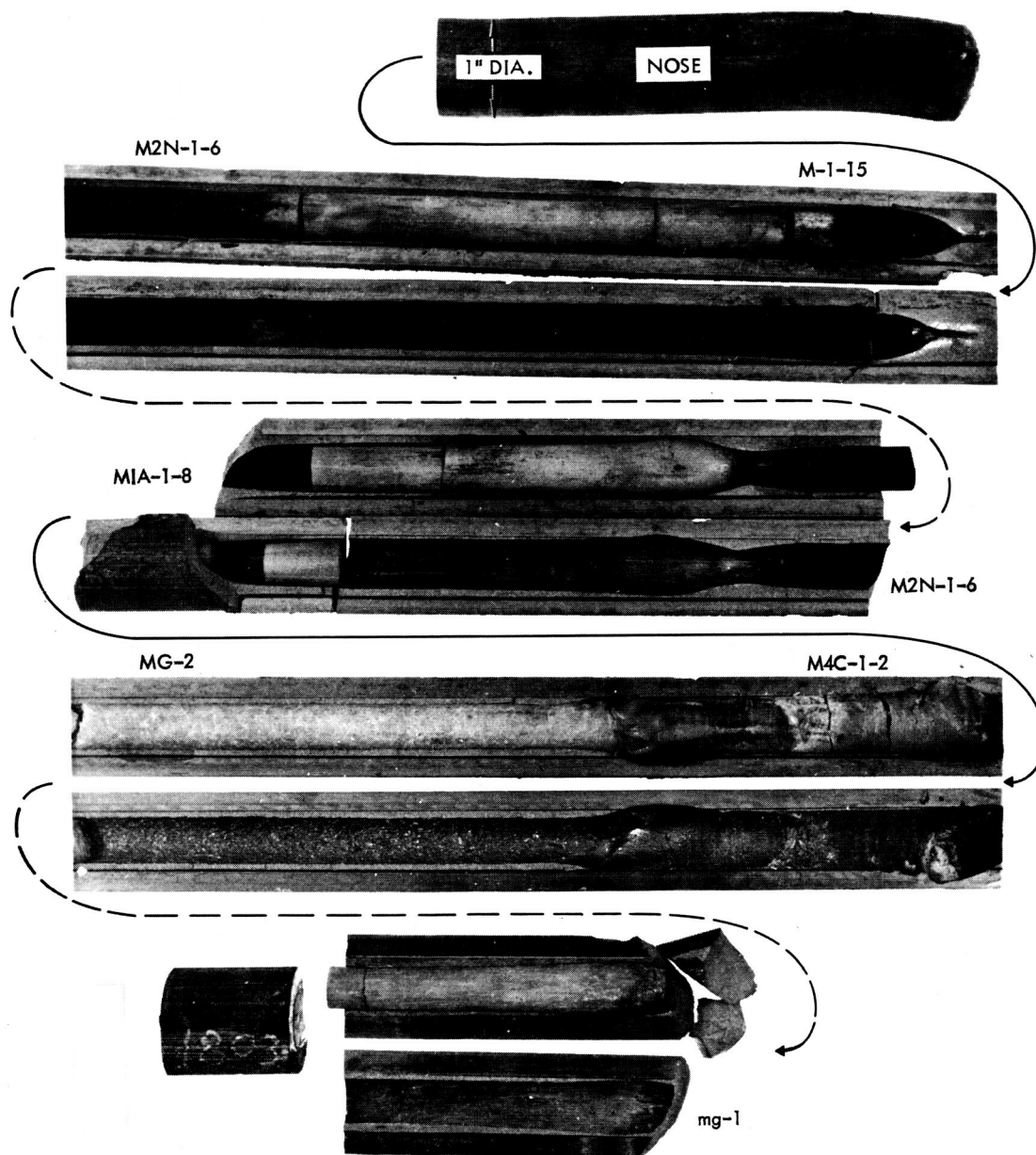
FIGURE 4   EXTRUSION MgO-6
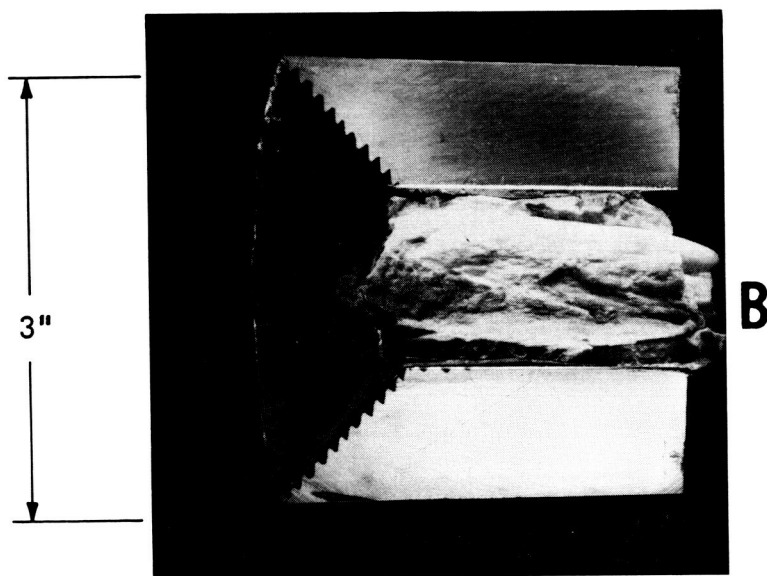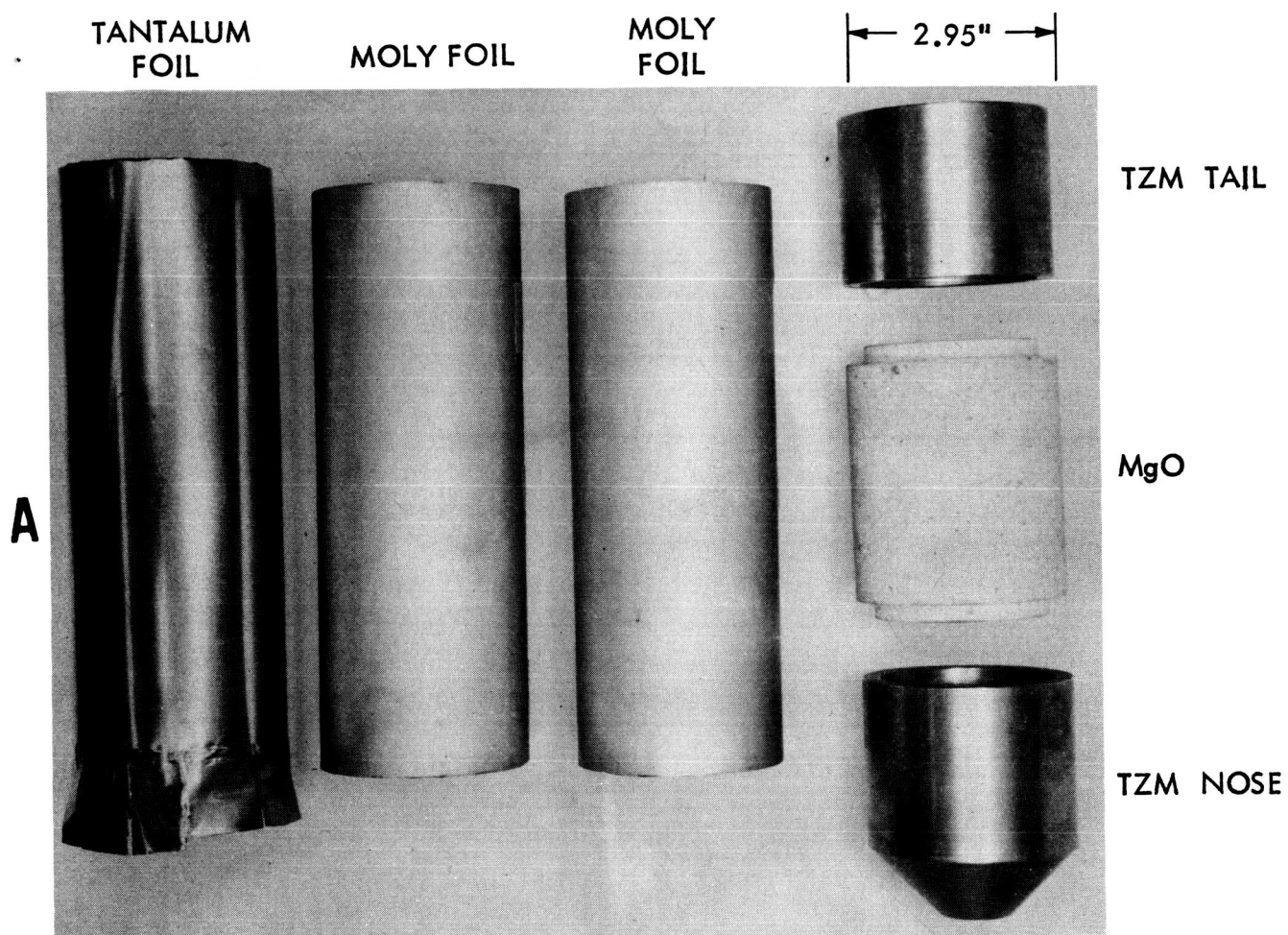
FIGURE 5 UNCANNED EXTRUSION: A) BREAKDOWN BEFORE ASSEMBLY AND EXTRUSION. B) PORTION STALLED IN DIE. (NOTE- DIE SERRATION TO HOLD ZrO_2 COATING. REDUCTION RATIO APPROXIMATELY 6 TO 1)
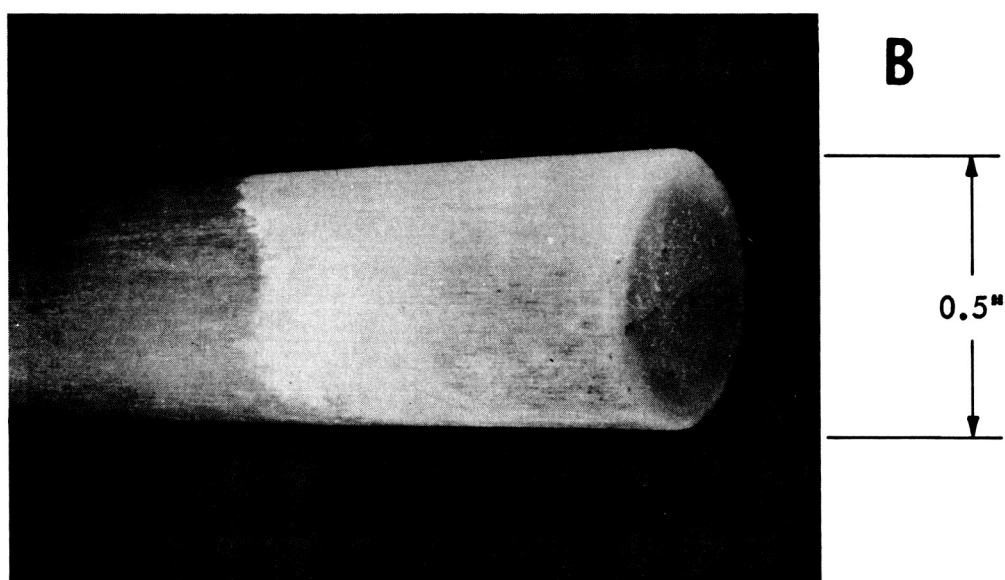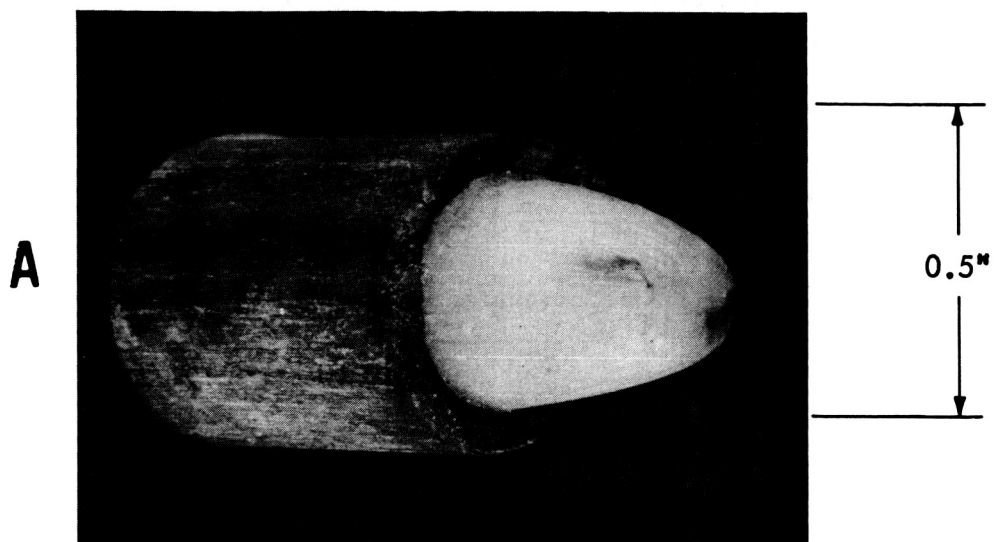
FIGURE 6 UNIFORM FLOW TRANSITION BETWEEN BILLETS. A) NOSE OF MIA-1-7 IN TAIL OF M 2 N-1-3 (MgO-2) B) NOSE OF M 2 N-1-3 IN TAIL OF M-1-6 (MgO-2)
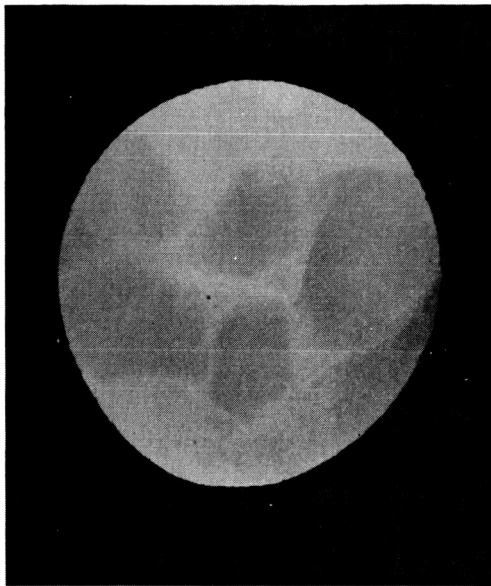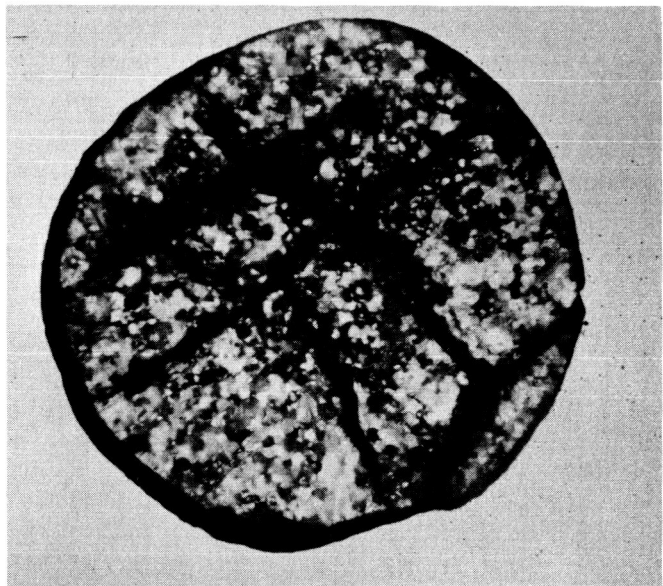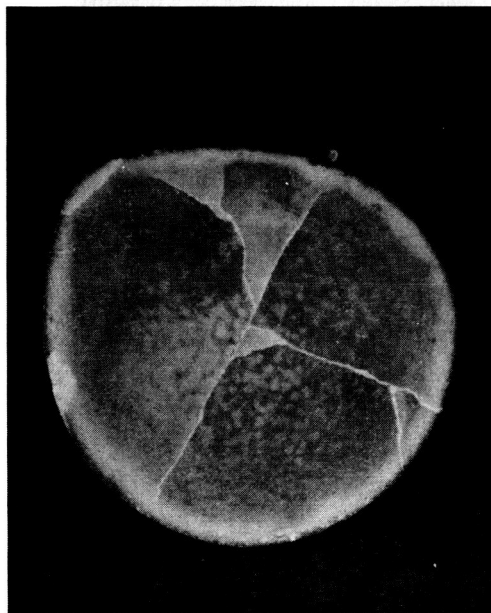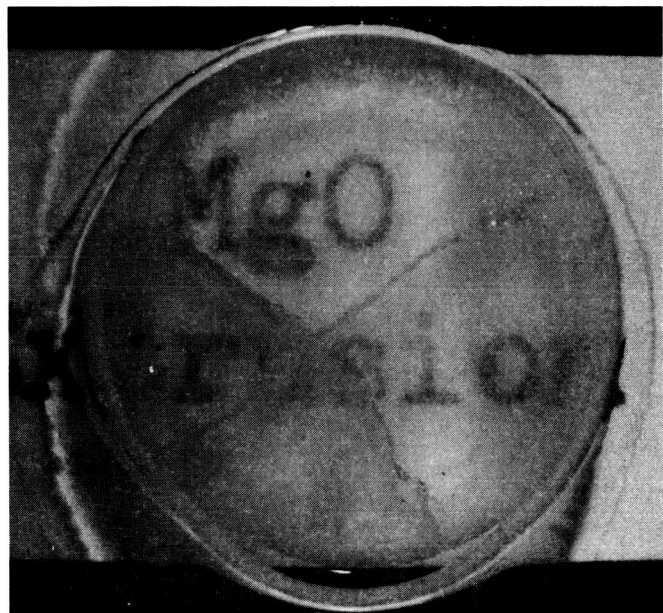
FIG. 7. EXTRUDED BILLET CROSS SECTION SAMPLES
    A) BILLET MIA-1-2 (MgO-3)
    B) M-f-3 (MgO-3)
    C) M2N-1-3 (MgO-2)
    D) M-1-7 (MgO-5) – THIS SPECIMEN IS SETTING IN A POOL OF GLYCERINE TO SHOW TRANSPARENCY. ALL SPECIMENS ARE APPROXIMATELY 0.5" IN DIAMETER.
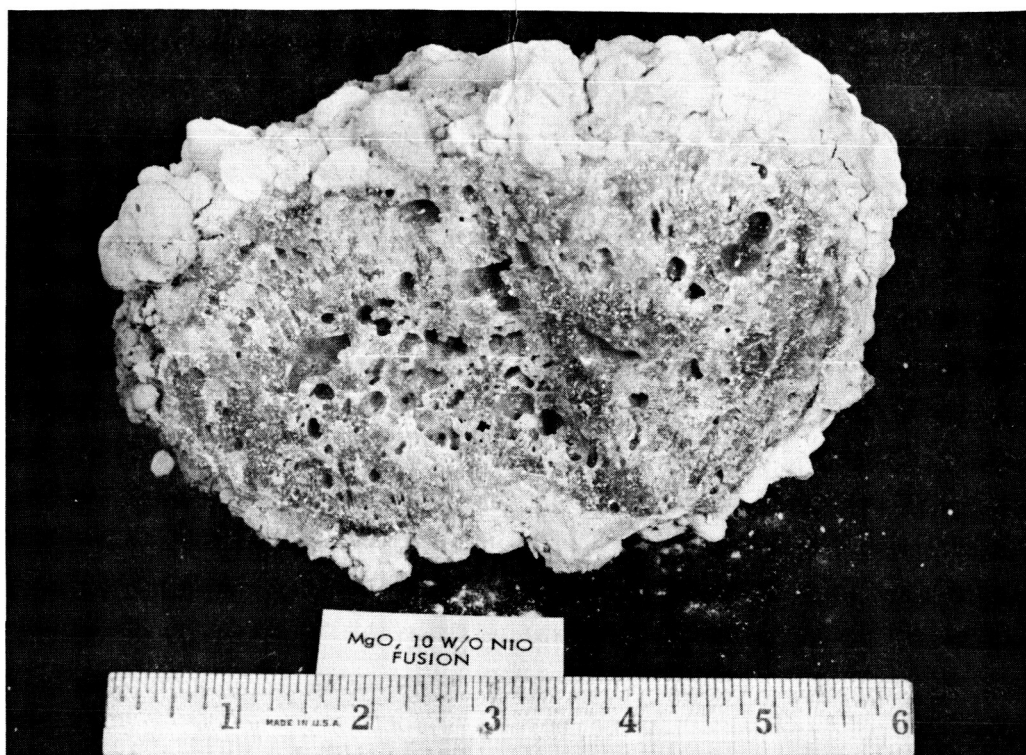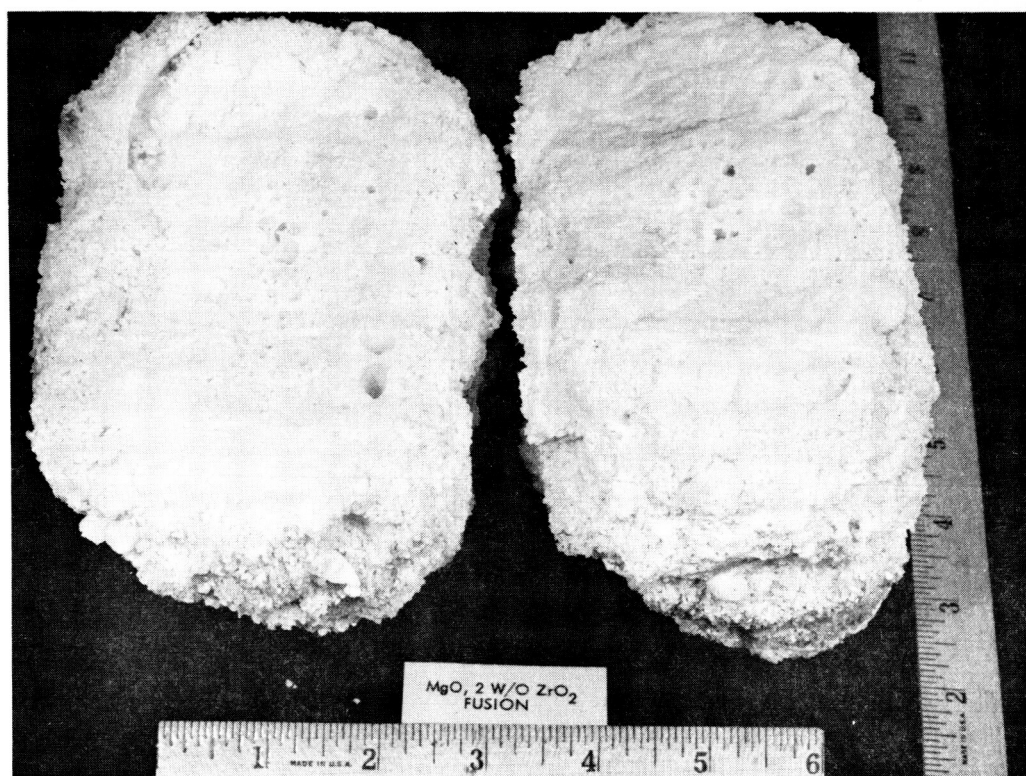
FIG. 8   FUSED INGOT SECTIONS A) MgO-10 $^{w}/_{o}$ NiO B) MgO-2 $^{w}/_{o}$ ZrO$_2$.
BILLETS CUT FROM OUTER, DENSER SECTIONS)
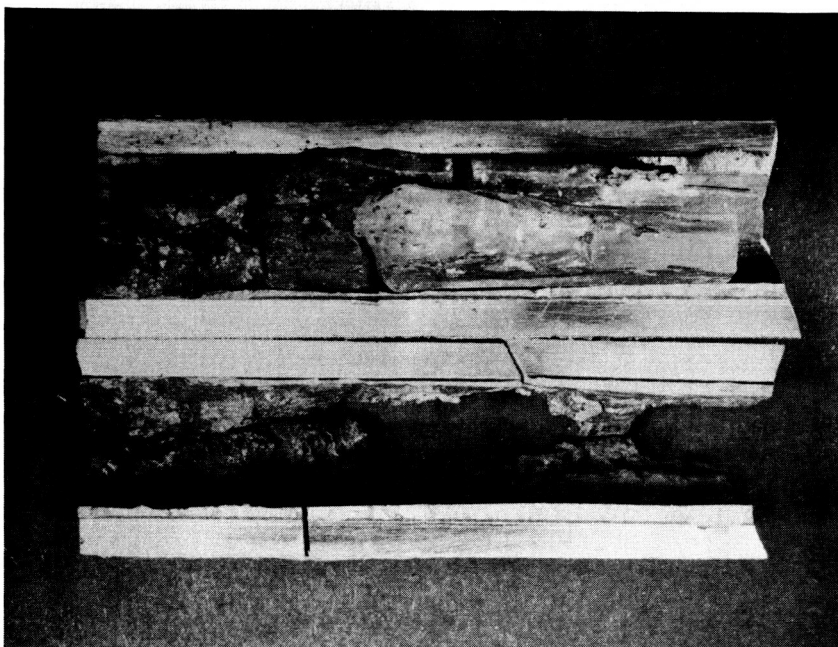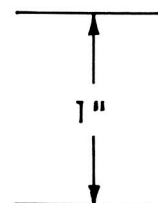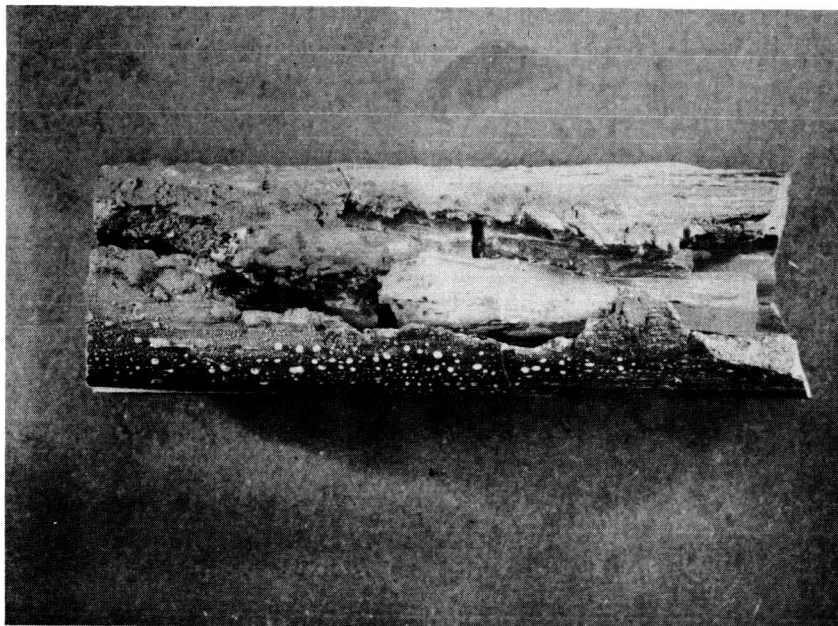
FIGURE 9   MgO BREAKING OUT OF CAN

0.1"
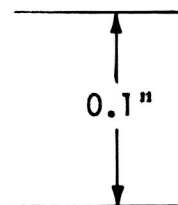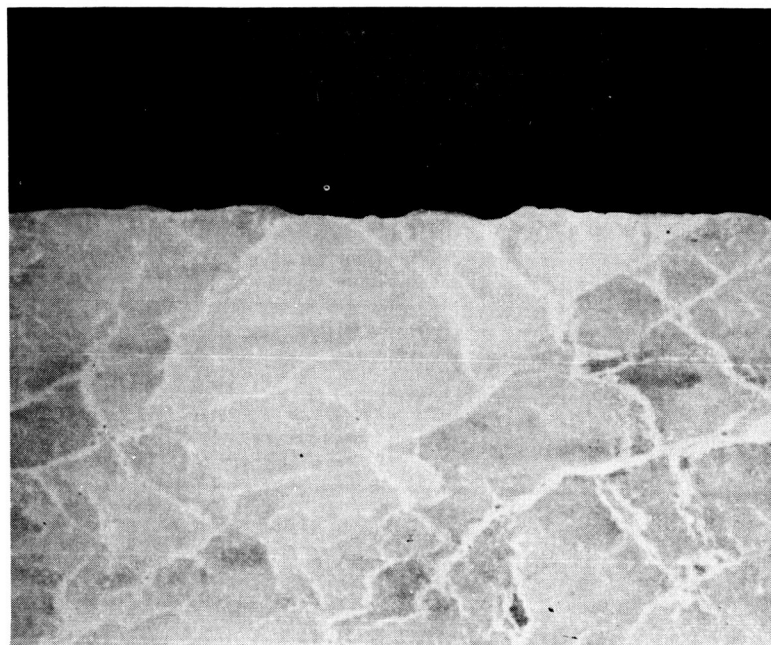
A
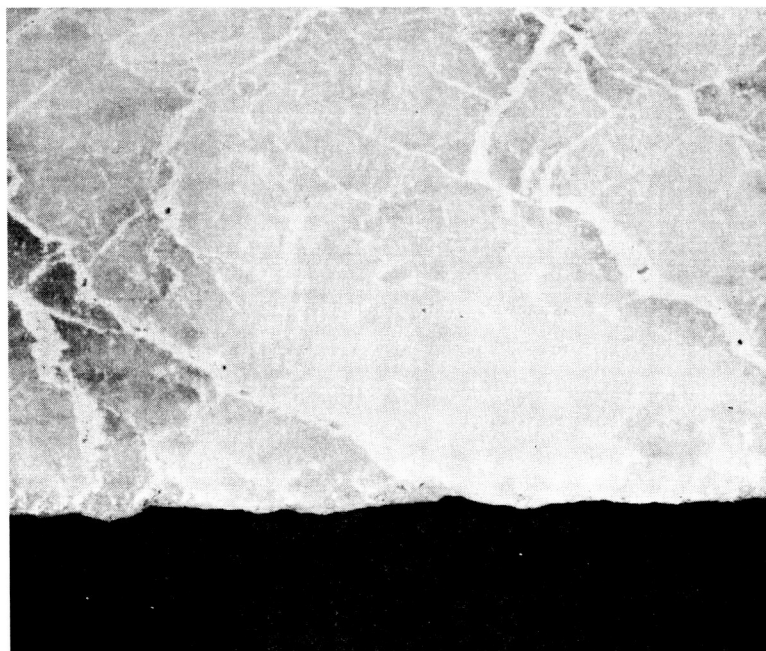
EXTRUSION DIRECTION ————————➤

FIG. 10 RANDOM AND LINEAR CRACKING
A) TWO EDGES OF MG-2 (MgO-6)

EXTRUSION
DIRECTION

→
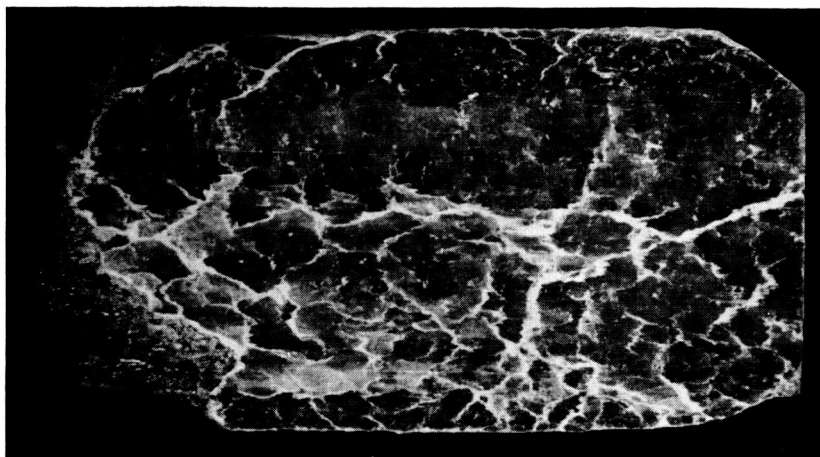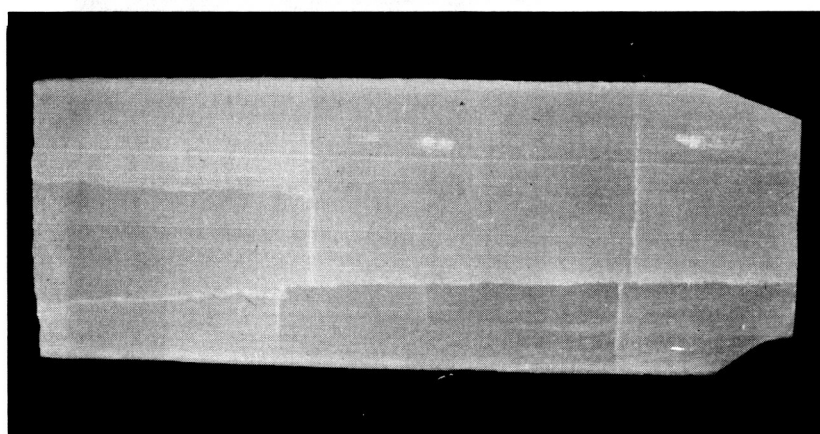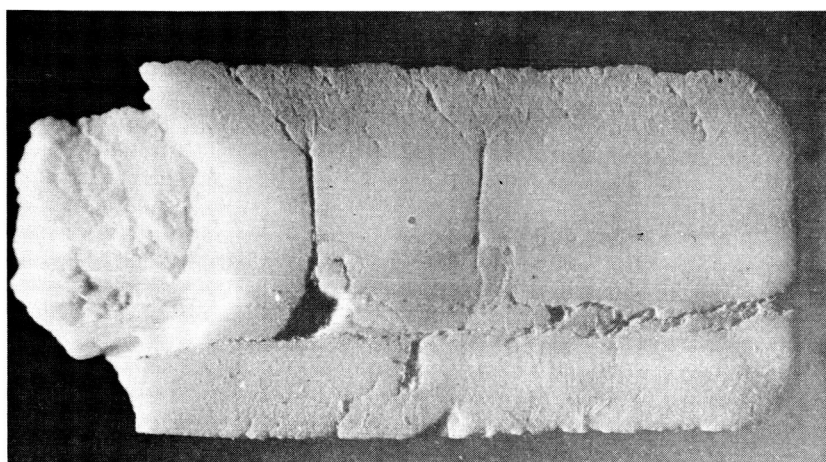
FIG. 10 RANDOM AND LINEAR CRACKING (CONT.)
   B) RANDOM CRACKING IN MION-1-1 (MgO-2)
   C) LINEAR CRACKING IN M-1-11 (MgO-5)
   D) INTERMEDIATE, M4C-1-4 (MgO-4)
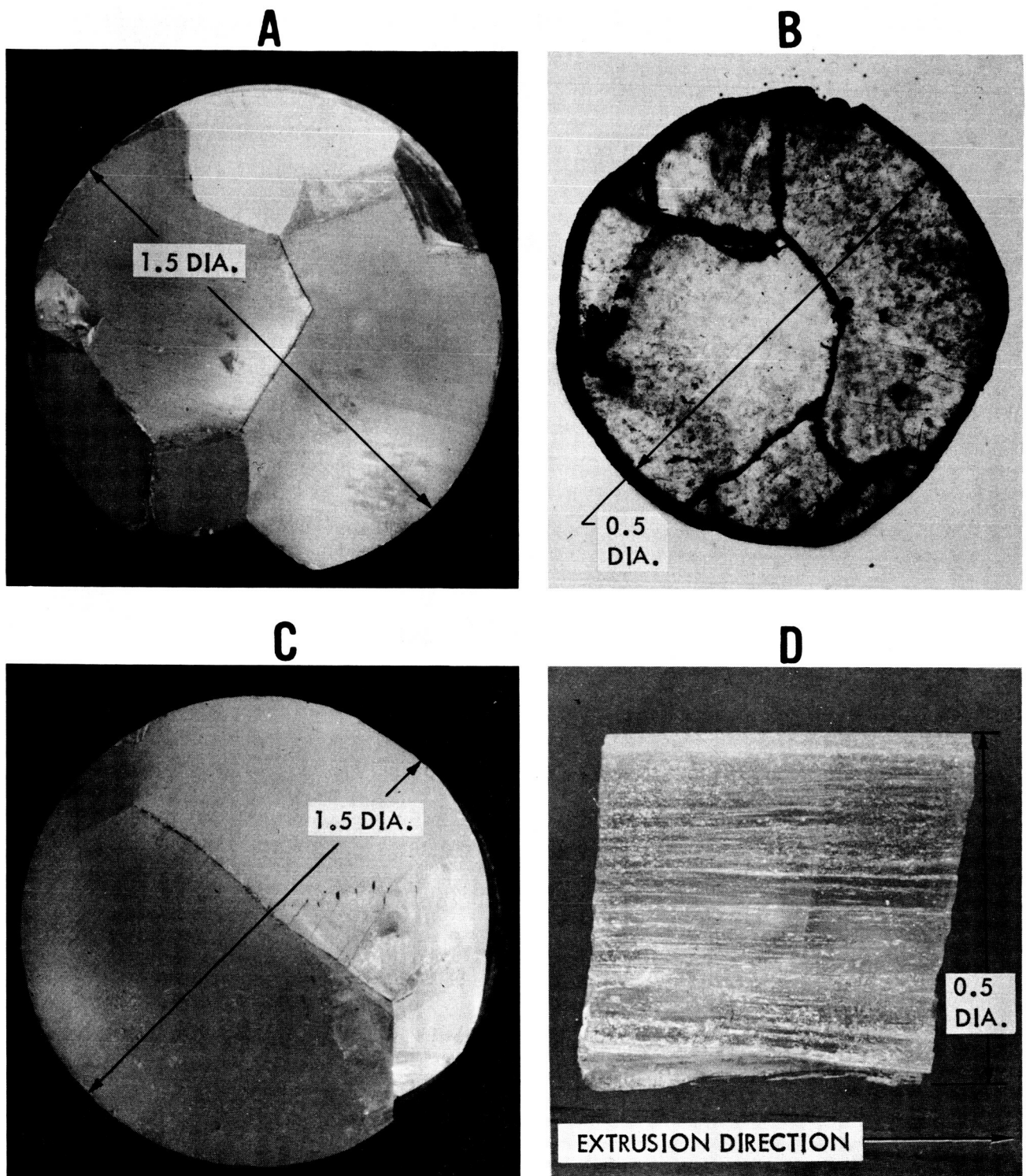
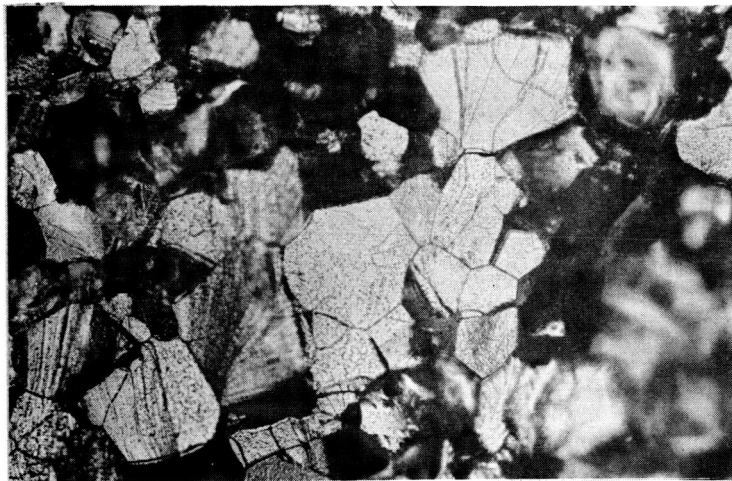ALL SPECIMENS ARE APPROXIMATELY 0.5" IN DIAMETER
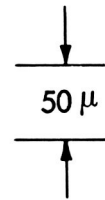
FIG. 11   FUSED GRAIN BOUNDARIES AND LONGITUDINAL CRACKING
          A) FRONT OF ORIGINAL FUSED BILLET M-f-5
          B) SECTION 2" BACK FROM FRONT OF EXTRUDED BILLET M-f-5
          C) REAR OF ORIGINAL FUSED BILLET M-f-4
          D) SURFACE OF LONGITUDINAL CRACK NEAR THE REAR OF EXTRUDED
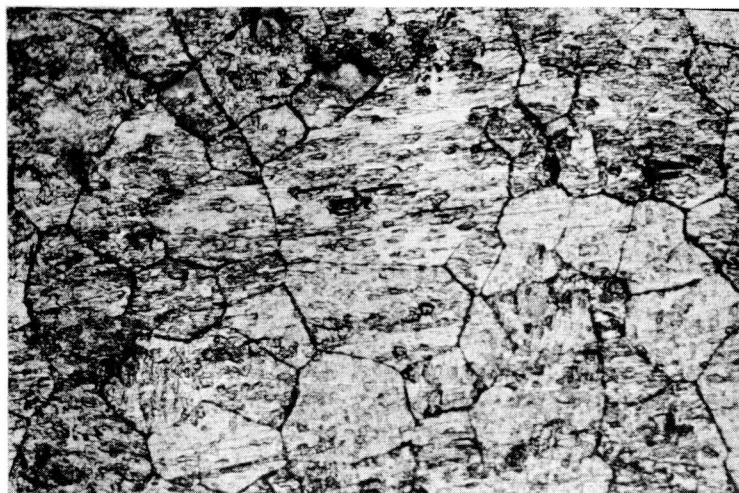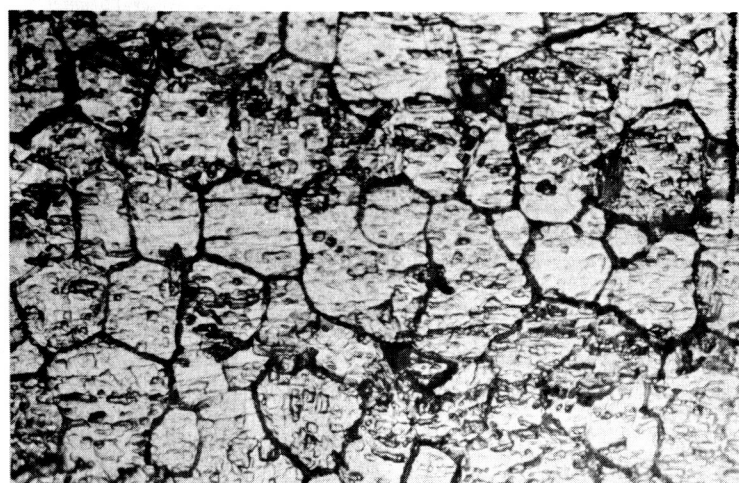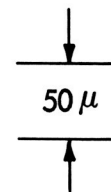   BILLET M-f-4

50 μ

FIG. 12 TYPICAL MICROSTRUCTURES, A) B) AND C):
TRANSVERSE SECTIONS (FRACTURES) OF BILLETS
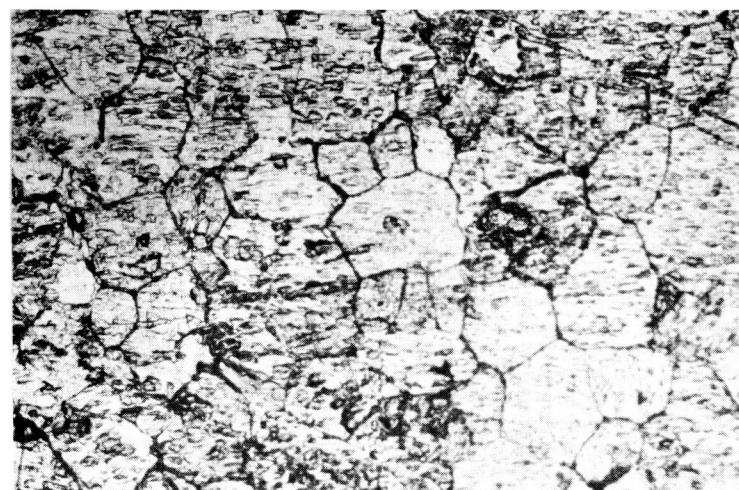M2N-1-2 (MgO-3), M-1-4 (MgO-4), AND M-1-12 (MgO-5) RESPECTIVELY

50 μ

EXTRUSION
DIRECTION
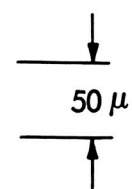
FIG. 12 (CONT.) TYPICAL MICROSTRUCTURES. D) E) AND F):
LONGITUDINAL SECTIONS OF BILLETS
M2N-1-2 (MgO-3), M-1-4 (MgO-4), AND M-1-12 (MgO-5) RESPECTIVELY
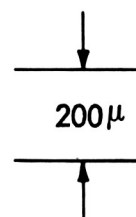
A

B

50 μ

FIG. 13 REDUCED SURFACE GRAIN SIZE.
A) TYPICAL CENTRAL GRAIN SIZE.
B) SURFACE GRAIN SIZE.
TRANSVERSE SECTION OF M-f-4 (MgO-2)

200 μ

EXTRUSION DIRECTION ⟶

FIG. 14 DISTINCT GRAIN SIZE VARIATION. LONGITUDINAL SECTION mg-1 (MgO-6)
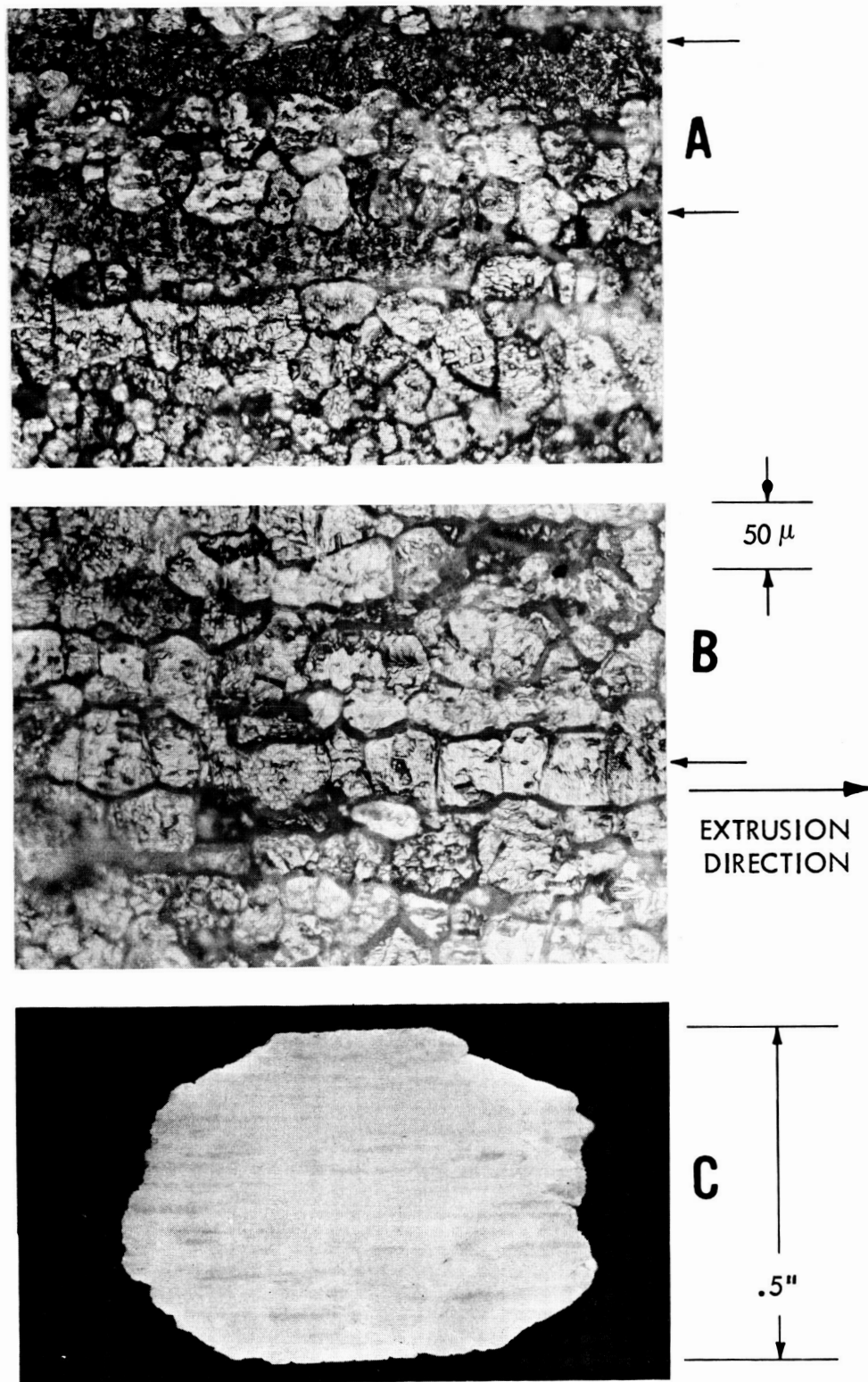
FIG. 15 GRAIN ELONGATION. LONGITUDINAL SECTIONS OF:
A) AND B) BILLETS M-1-6 (MgO-2) AND M-1-14 (MgO-5) (NOTE SMALL
ARROWS INDICATING ELONGATED GRAINS OR THEIR PROBABLE REMNANTS)
C) BILLET MG-3 (MgO-5) (NOTE DARK, ELONGATED PATCHES - PROBABLE
ELONGATION OF ORIGINAL LARGE DENSE MgO GRAINS (FUSED) - THESE
WERE RECRYSTALLIZED).

A

B

50 μ
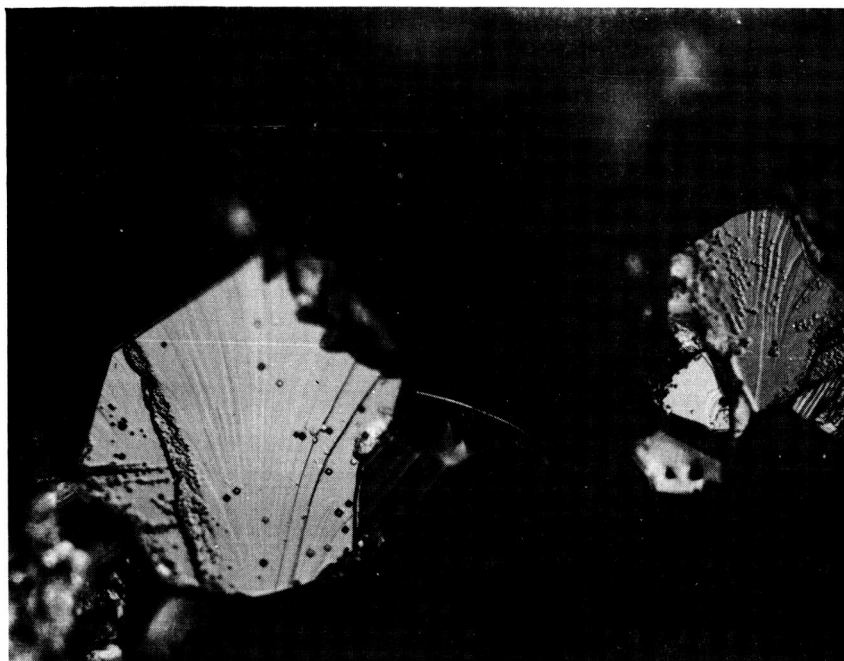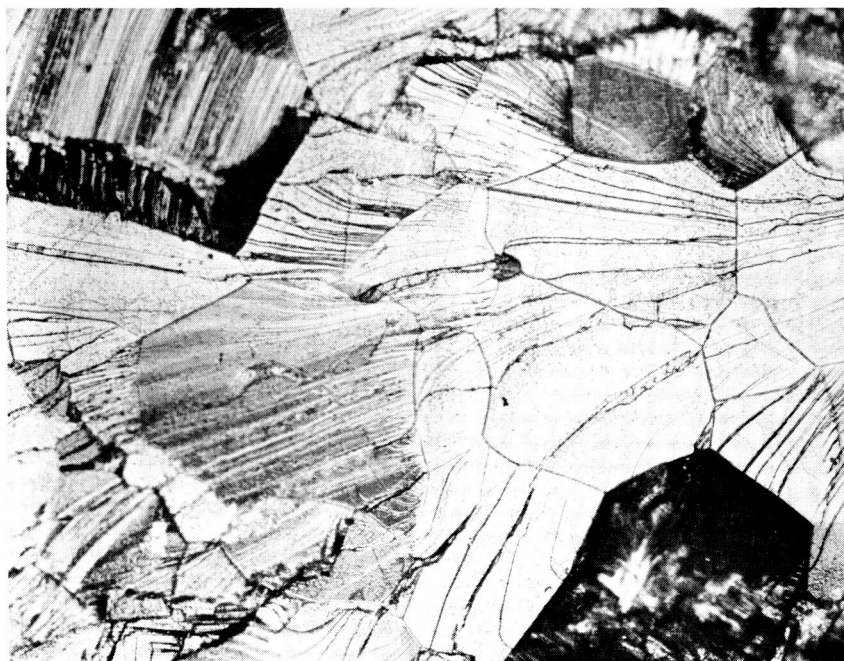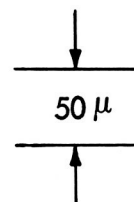
FIG. 16 CONTRAST IN TRANSVERSE FRACTURE OF EXTRUDED AND UNEXTRUDED MgO.
A) BILLET M-f-5 (MgO-5)   B) UNEXTRUDED MgO BODY FABRICATED
PER VACUUM HOT PRESSING PROCEDURE B AND FIRING SCHEDULE A.
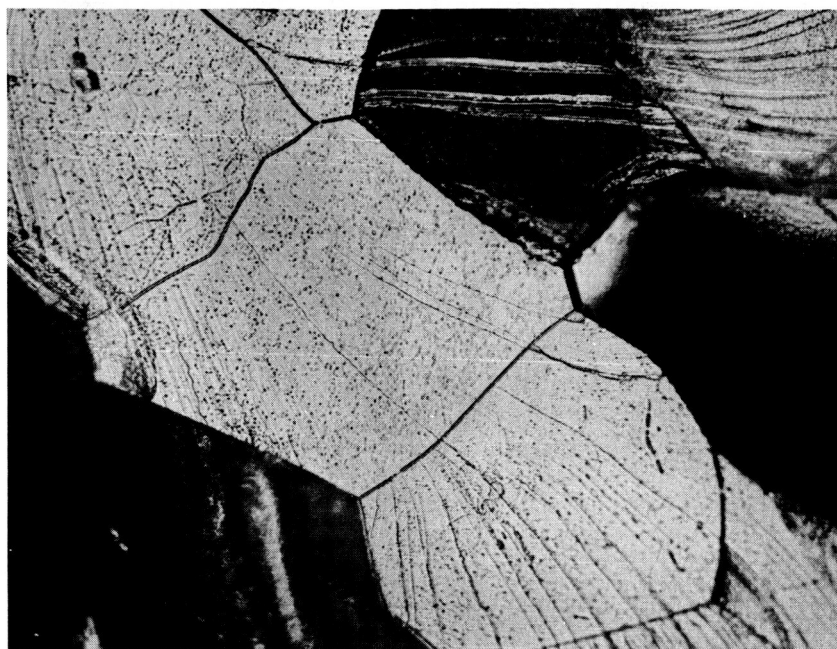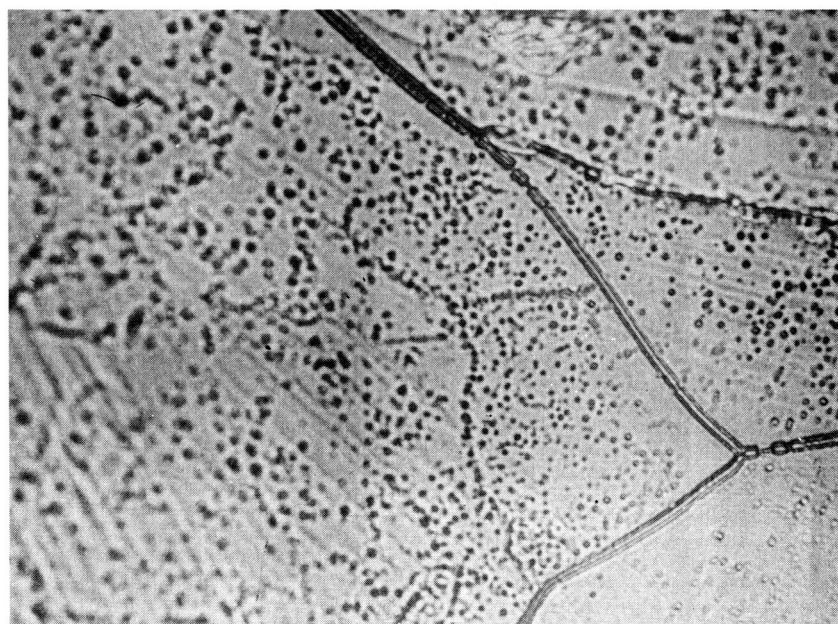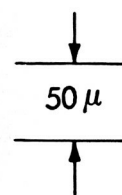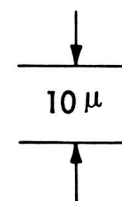
FIG. 17 SUB-BOUNDARIES IN EXTRUDED BODIES.
SAMPLE: TRANSVERSE FRACTURE OF M-f-3 (MgO-3)
A) AND B) FROM THE SAME AREA
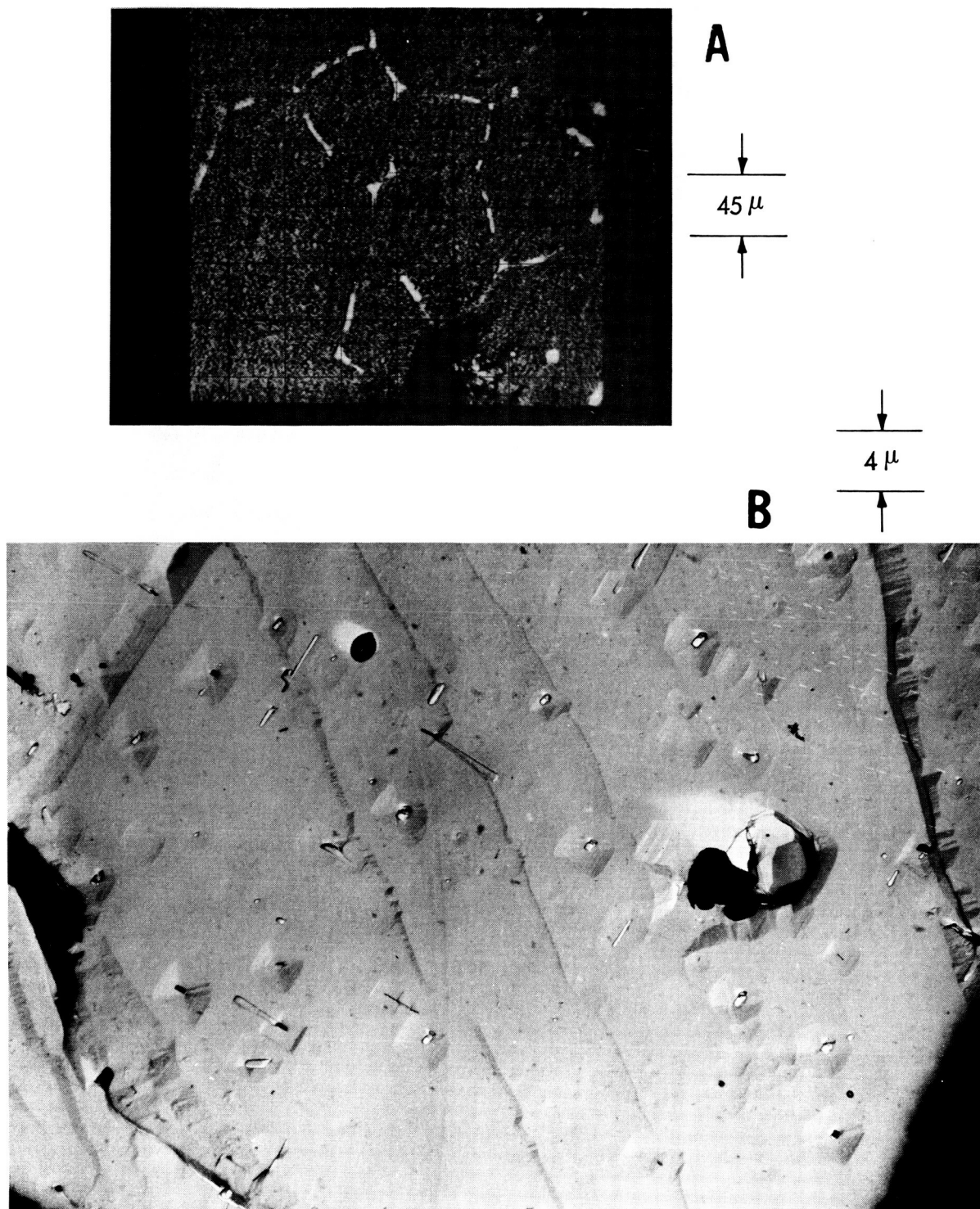
FIG. 18 MgO-2 w/o ZrO$_2$ FUSION ANALYSIS. AS RECEIVED INGOT:
A) ELECTRON PROBE ANALYSIS - WHITE: ZrO$_2$ RICH, GRAY:
MgO, BLACK: VOID, CRACK OR GRAIN PULL-OUT.
B) ELECTRON MICROGRAPH OF FRACTURE SURFACE ETCHED IN
BOILING CHROMIC ACID.
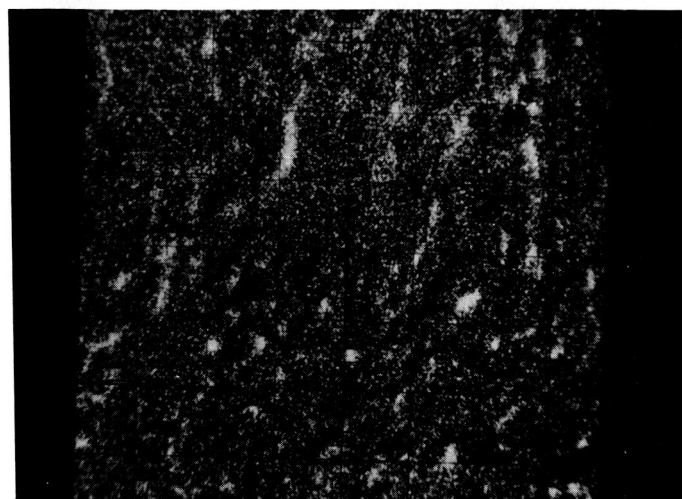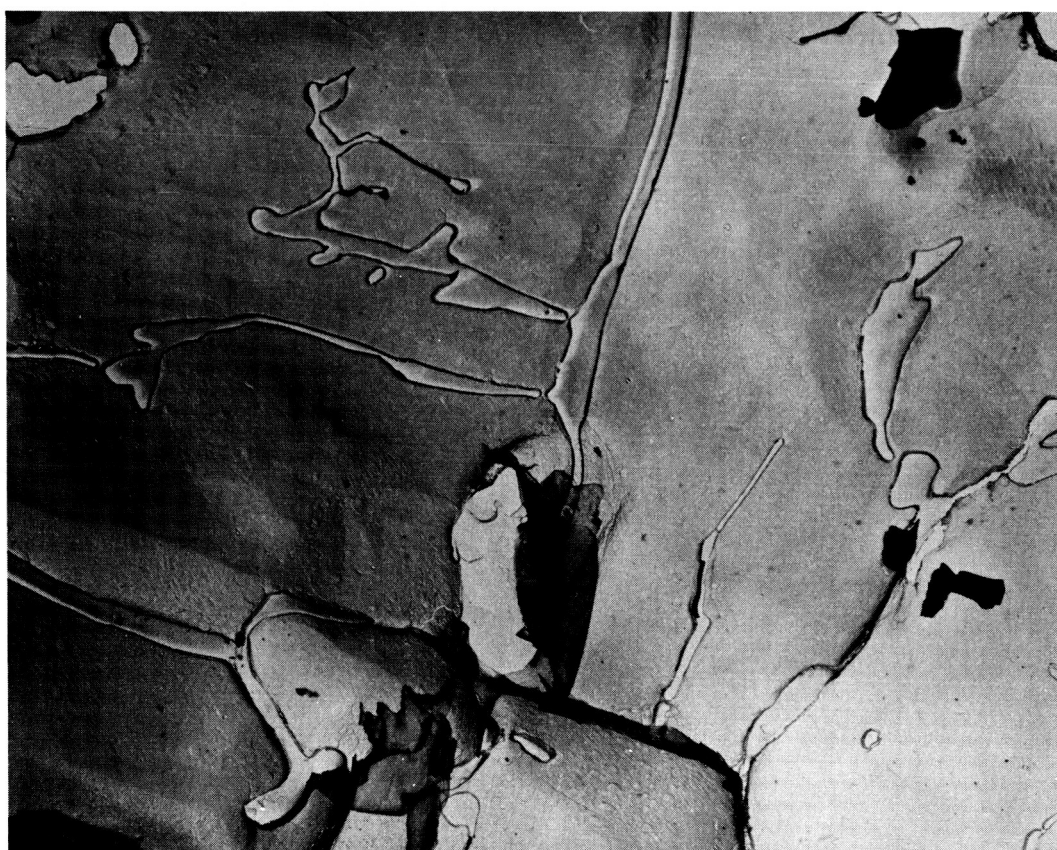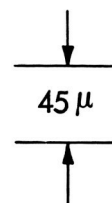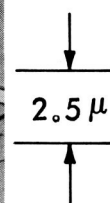
FIG. 19 EXTRUDED BILLET M2Z-1-3 ANALYSIS. A) ELECTRON PROBE
ANALYSIS - WHITE AREAS ZrO_2 RICH, GRAY - MgO   B) ELECTRON
MICROGRAPH OF FRACTURE SURFACE ETCHED IN BOILING CHROMIC
ACID.

TABLE I   BILLET FABRICATION

Billet Number	Composition	Fabrication	Firing Schedule	Density gm/cc [1]
M-f-6	MgO	Fusion		laminated
M-f-7				
M-f-8				
M-1-19	Fisher MgO	Per Vacuum Hot Pressing Procedure B	A to 1565°C(2850°F)	3.49
M-1-20				broke die
M-2-1				ram broke
M-2-2				broke die
M-2-3				
M-2-4				3.58
M-2-5				3.47
M5N-1-1	$MgO-5\ ^w/_o NiO$	See Text	A to 1565°C(2850°F)	3.27
M5N-1-2				broke die
M5A-1-1	$MgO-5\ ^w/_o Al_2O_3$	See Text	A to 1565°C(2850°F)	3.40
M2Z-1-6	$MgO-2\ ^w/_o ZrO_2$	Per Vacuum Hot Pressing Schedule B	A to 1565°C(2850°F)	3.59
C-1-4	CaO	"	A to 1565°C(2850°F)	3.15
Ce-1-1	CeO_2	Isostatic Pressing (see text)	1565°C(2850°F) – see text	6.62
Ce-1-2	CeO_2			6.82
Sma-1-1	$MgAl_2O_4$	Fusion		3.21
Sma-1-2				
Z-1-1	ZrO_2	Purchased		5.40

[1] Nominal density error is ± 0.01 gm/cc.

39

TABLE II EXTRUSION PARAMETERS

Extrusion Number	Initial Ceramic Diameter (Inches)	Initial Can Wall Thickness	Temperature °C [1]	Area Reduction Ratio [2]	Speed In/sec.	Upset Force (tons) [3]	Running Force Start (tons) [4]	End (tons) [5]
MgO-2	1.5	0.75	2100	9 to 1	1.7	550	450	630 [6]
MgO-3	1.5	0.75	2200	9 to 1	10	545	420	520
MgO-4	1.5	0.75	2300	9 to 1	11	520	450	550
MgO-5	1.5	0.75	2200	9 to 1	11	535	430	500
MgO-6	1.5	0.75	2400	9 to 1	10	500	450	450
Uncanned Extrusion	2.95	0.05	2300	6 to 1	5-15	600	400	500 – 600 [7]

[1] Temperature of Composite billet on dropping from furnace.

[2] Area Reduction Ratio decreases with die erosion. This may reduce the ratio to the order of 8 to 1 In some cases.

[3] Force to extrude tungsten nose.

[4] Force to extrude first ceramic section.

[5] Force to extrude last ceramic section.

[6] Extrusion stalled at end of last ceramic section.

[7] Extrusion stalled at 600 tons.

40

TABLE III   EXTRUDED BILLET DATA
CERAMIC BILLET

Extrusion: Number / Temperature / Area reduction ratio [1]	Number	Composition	Fabrication [2]	Density Before Extrusion [3]	Density After Extrusion (gm/cc) [4]	Area Reduction Ratio	Avg Grain Size (Microns) Transverse [5]	Avg Grain Size (Microns) Longitudinal	Orientation Maximum High [6]	Orientation Maximum Low	Orientation Maximum Average
MgO-1 2150°C 8 to 1	M-f-1	MgO	Fusion			5-14 to 1	180	220	40	30	35
	M1A-1-1	$MgO-1^w/_oAl_2O_3$	A		3.48	6-8 to 1		40	15	5	10
	M5C-1-1	$MgO-5^w/_oCaO$	Fusion			6 to 1	50		44	35	40
	M2N-1-1	$MgO-2^w/_oNiO$	A		3.52	4.5-7.5 to 1		40			
MgO-2 2100°C 9 to 1	M-f-4	MgO	Fusion			8-9 to 1	100	160	64	33	45
	M-1-6	MgO	A	3.54		8-9 to 1	30	40	59	54	56
	M2N-1-3	$MgO-2^w/_oNiO$	A	3.40	3.60	8-9 to 1	40	40	63	55	59
	M1A-1-7	$MgO-1^w/_oAl_2O_3$	A	3.49		8-9 to 1	30	30	42	37	39
MgO-3 2200°C 9 to 1	M-f-3	MgO	Fusion			8-9 to 1	200	300	78	2	40
	M-1-1	MgO	A	3.52		8-9 to 1	70	90	50	59	53
	M-1-2	MgO	A			8-9 to 1	80				
	M-1-5	MgO	A			8-9 to 1	80				
	M-1-10	MgO	B	3.53	3.57	8 to 1	50	40			
	M2N-1-2	$MgO-2^w/_oNiO$	A			8 to 1	75	90			
	M1ON-1-1	$MgO-10^w/_oNiO$	Fusion			8-9 to 1	80	90	62	52	59
	M1A-1-2	$MgO-1^w/_oAl_2O_3$	A			8-9 to 1	50	70	56	48	52
	M1A-1-3	$MgO-1^w/_oAl_2O_3$	A			8 to 1	60	70	21	9	14
MgO-4 2300°C 9 to 1	M2Z-1-1	$MgO-2^w/_oZrO_2$	Fusion		3.53	7-9 to 1	50	20	35	17	24
	M2Z-1-3	$MgO-2^w/_oZrO_2$	B	3.55	3.54	8-9 to 1	70	30	18	8	12
	M-1-4	MgO	A	3.26		8-9 to 1	75	90	35	30	32
	M5C-1-2	$MgO-5^w/_oCaO$	Fusion			7-9 to 1		20	8.6	3.3	6.5
	M4C-1-4	$MgO-4^w/_oCaO$	B	3.43	3.46	7-9 to 1	20		6.5	4.5	6.0
	M4C-1-1	$MgO-4^w/_oCaO$	B	3.37		4-5 to 1		40	18	12	16

TABLE III (Cont.) EXTRUDED BILLET DATA
CERAMIC BILLET

Extrusion: Number Temperature Area reduction ratio [1]	Number [1]	Composition	Fabrication	Density gm/cc Before Extrusion [2]	Density gm/cc After Extrusion [3]	Area Reduction Ratio [4]	Avg Grain Size (Microns) [5] Transverse	Avg Grain Size (Microns) [5] Longitudinal	Orientation Maximum [6] High	Orientation Maximum [6] Low	Orientation Maximum [6] Average
MgO-5 2200°C 9 to 1	M-f-5	MgO	Fusion			8-9 to 1	130	130			
	M-1-7	MgO	A	3.55	3.59		60	60	57	43	**50**
	M-1-11	MgO	B	3.54	3.58		70	60	62	42	53
	M-1-14	MgO	B	3.55	3.56		30	30	25.5	12	20
	MG-3	MgO	G	2.74		8-10 to 1	60	80	11	5.5	7.0
	MG-1	MgO	G	2.60		8-10 to 1	70	80	70	60	**68**
	M-1-12	MgO	B	3.56		8-9 to 1	40	50	61	55	**58**
	M-1-15	MgO	B	3.45	3.58	8-9 to 1	40	40	56	49	52
MgO-6 2400°C 9 to 1	M2N-1-6	MgO-2w/oNiO	A		3.62	9-10 to 1	40	50	41	30	37
	M1A-1-8	MgO-1w/oAl$_2$O$_3$	A	3.53	3.57	7-9 to 1	60		3.7	1.9	2.8
	M4C-1-2	MgO-4w/oCaO	B			4-7 to 1	20	20	7.0	3.0	5.0
	MG-2	MgO	G	2.74		9 to 1	30		46	38	**40**
	mg-1	MgO	g		3.58	11 to 1		80			

[1] Billets are listed front to rear from the top.

[2] A and B refer to vacuum hot pressing procedures or modifications as noted in reference 3, G refers to billets made from MgO grain -- see reference 3, g refer to grain loaded in the tungsten can.

[3] ±0.01 gm/cc.

[4] ±0.02 gm/cc. Extensive internal cracking will reduce density.

[5] Estimated grain size.

[6] Orientation maximum is determined by the ratio of the peak intensity of the 200 plane (at or near the extrusion axis) in comparison to a random sample. The average is obtained from a strip chart recorder run while the specimen (transverse section) is oscillated perpendicular to the plane of the X-ray beam.

TABLE IV ESTIMATE GRAIN SIZE JUST PRIOR TO EXTRUSION

Composition	Fabrication	Grain Size Range Due to Heating For Extrusion
MgO	Fusion	1 to 5 centimeters
MgO	Solid state [1]	200 – 800 microns
MgO – NiO	Fusion	200 – 1000 microns
MgO – NiO	Solid state	100 – 400
MgO – Al_2O_3	Solid state	200 – 800
MgO – CaO	Fusion	500 – 2000
MgO – CaO	Solid state	50 – 200
MgO – ZrO_2	Fusion	50 – 500
MgO – ZrO_2	Solid state	100 – 600

[1] Solid state refers to any combination of pressing and firing short of fusion as discussed in previous reports (1)(3). The range of grain size in hot pressed billets after firing on Firing Schedule A will generally be between one half of the lower value and one third of the higher values shown for the corresponding body.

APPENDIX
CALCINING PROCEDURE A

1. Powder is loaded in 99% pure MgO crucibles approximately 3" in diameter x 4" high with 0.1" wall thickness by using the crucible to scoop powder from the container.

2. The crucibles are placed in a metal retort with half of them inverted on top of the remainder. The top crucibles are slotted on the side near their base to allow ready gas escape and good flushing while acting as lids to prevent excess spillage of powder, and possible contamination from the retort metal lid.

3. A thin metal lid is welded on the retort to seal it.

4. Lines are attached to fittings to introduce argon at the bottom in front, and a vacuum system to the top of the retort in the back.

5. The retort is loaded in the furnace and the vacuum and argon valves are set to establish an argon flush at about 10" absolute pressure.

6. The retort is heated at a linear rate to reach 600°C (1110°F) in approximately 5.5 hours. Temperatures are measured by a thermocouple near the center of the retort.

7. After 1 hour at 600°C, the retort is cooled in approximately 1.5 hours, initially in the furnace, then out of the furnace.

8. When the retort is less than 100°C the vacuum valve is closed, when the retort is near atmosphere pressure, the argon valve is closed, and the retort is flooded with benzene through a third fitting.

9. The thin retort lid is then removed and the powder, covered with benzene, is transferred to jars which are closed for storage.
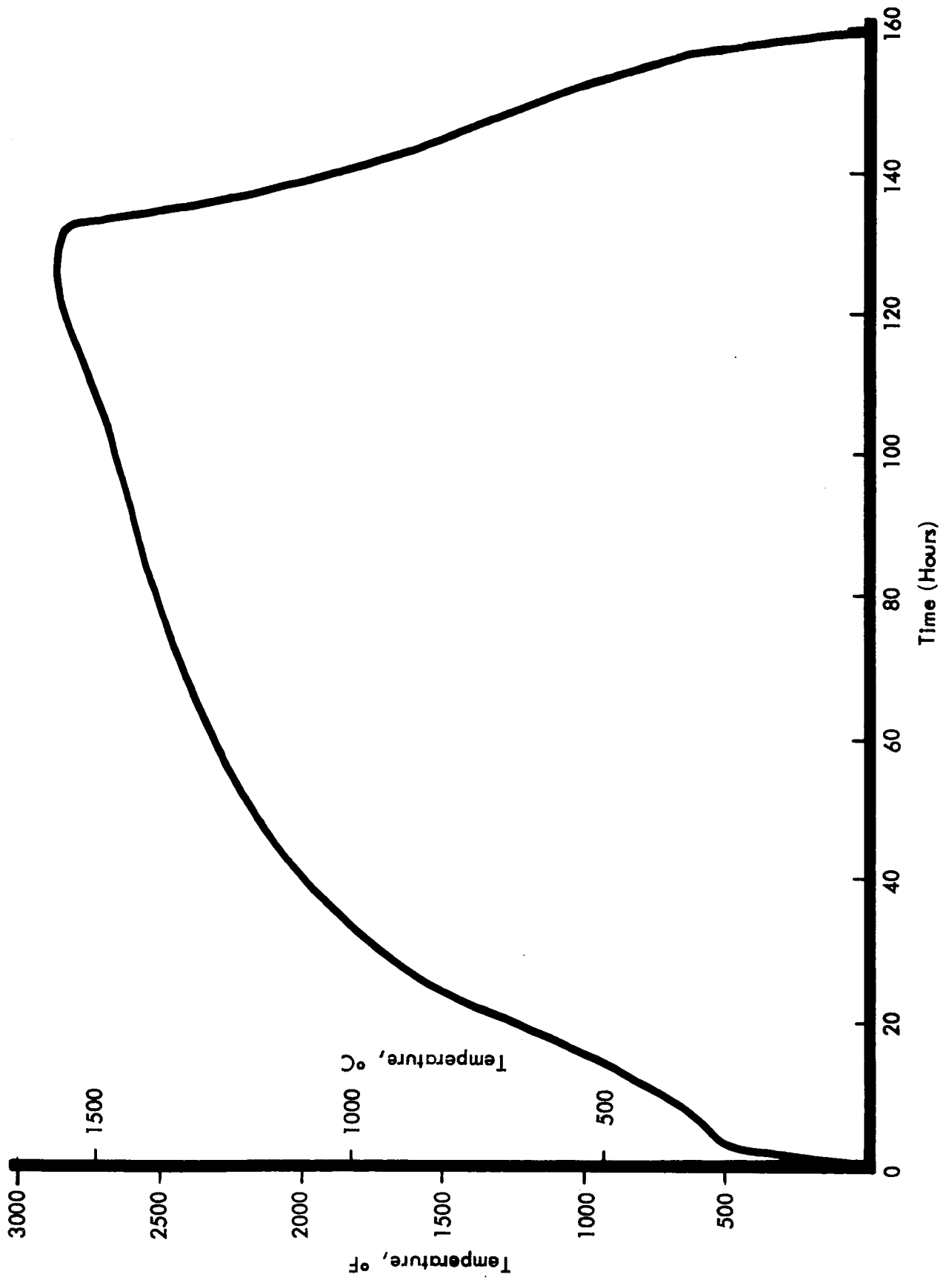
APPENDIX
BILLET VACUUM HOT PRESSING PROCEDURE A (WITH LiF)

1. Two weight per cent reagent grade LiF is added to the ceramic powder by milling for 2 hours in an organic fluid, normally benzene.

2. The milled slurry is dried, screened through a number 28 screen, and stored in sealed jars. The time of storage in sealed jars is normally less than one week prior to complete usage of the powder.

3. Powder is loaded in the die by cold pressing at 1000-2000 psi. Pyrolytic graphite spacers are placed between the rams and the powder when graphite dies are used.

4. The die is placed in the vacuum hot press which is pumped down to a chamber pressure of 10^{-4} - 10^{-5} Torr in about 1 hour.

5. After at least 4 hours at 10^{-4} - 10^{-5} Torr, the die is heated at an approximately linear rate to 650°C (1200°F) in about 0.5 hour. Temperatures are measured by a thermocouple in the die wall approximately 0.75" from the inside die surface and about 1" above the specimen.

6. Between 650°C and 700°C the ram pressure is built up to approximately 3500 psi.

7. Heating, while maintaining this ram pressure, is continued at a slightly slower rate until a temperature of 980°C (1800°F) is reached after a total heating time of 50 to 60 minutes.

8. Pressing conditions of 980°C and 3500 psi are held for 15 minutes with vacuum chamber pressure averaging 2 to 4 x 10^{-3} Torr.

9 The heating power is shut off and the ram pressure released over a period of about 1 minute.

10. The die is removed from the vacuum hot press after 2 to 4 hours of cooling.

11. The specimen is ejected from the die at temperatures of 400°C or less.

1. Powder is directly loaded into the die from sealed bottles, without any prior milling unless milling was previously used to mix alloy agents. Pyrolytic graphite spacers are used between the rams and the specimen when graphite dies are used.

2. The powder is cold pressed at 1000-2000 psi.

3. The die is placed in the vacuum hot press which is pumped down to a chamber pressure of 10^{-4} to 10^{-5} Torr in about one hour.

4. After at least 6 hours at 10^{-4} - 10^{-5} Torr the die is heated to 900°C (1650°F) in about 30 minutes. Temperatures are measured by a thermocouple located in the die wall about 0.75" from the inside die surface and about 1" above the specimen.

5. Starting at 900°C the ram pressure is built up to 5000 psi over a period of about 2 minutes.

6. A temperature of 1205° (2200°F) is then reached in about 20 minutes, while maintaining the ram pressure at 5000 psi.

7. Pressing conditions of 1205°C and 5000 psi are held for 15 minutes with vacuum chamber pressure averaging about 10^{-2} Torr.

8. The induction heating power is shut off and the ram pressure released over a period of about 1 minute.

9. The die is removed from the vacuum hot press after cooling for two to four hours.

10. The specimen is ejected from the die at a temperature of 400°C or less.

Temperature, °C

Temperature, °F

Time (Hours)

FIRING SCHEDULE A